https://doi.org/10.1093/plphys/kiac601 PLANT PHYSIOLOGY 2023: 192: 469–487

Plant Physiology®

Research Article

# Abscisic acid increases hydrogen peroxide in mitochondria to facilitate stomatal closure

**Anthony E. Postiglione and Gloria K. Muday***

Department of Biology and the Center for Molecular Signaling, Wake Forest University, Winston Salem, North Carolina, USA 27109

*Author for correspondence: muday@wfu.edu (G.K.M.)

A.E.P. designed experiments, performed research, analyzed data, and wrote the paper. G.K.M. designed experiments, wrote, and edited the paper. The author responsible for distribution of materials integral to the findings presented in this article in accordance with the policy described in the Instructions for Authors (https://academic.oup.com/plphys/pages/general-instructions) is Gloria K. Muday (muday@wfu.edu).

## Abstract

Abscisic acid (ABA) drives stomatal closure to minimize water loss due to transpiration in response to drought. We examined the subcellular location of ABA-increased accumulation of reactive oxygen species (ROS) in guard cells, which drive stomatal closure, in Arabidopsis (*Arabidopsis thaliana*). ABA-dependent increases in fluorescence of the generic ROS sensor, dichlorofluorescein (DCF), were observed in mitochondria, chloroplasts, cytosol, and nuclei. The ABA response in all these locations was lost in an ABA-insensitive quintuple receptor mutant. The ABA-increased fluorescence in mitochondria of both DCF- and an $H_2O_2$-selective probe, Peroxy Orange 1, colocalized with Mitotracker Red. ABA treatment of guard cells transformed with the genetically encoded $H_2O_2$ reporter targeted to the cytoplasm (roGFP2-Orp1), or mitochondria (mt-roGFP2-Orp1), revealed $H_2O_2$ increases. Consistent with mitochondrial ROS changes functioning in stomatal closure, we found that guard cells of a mutant with mitochondrial defects, *ABA overly sensitive 6* (*abo6*), have elevated ABA-induced ROS in mitochondria and enhanced stomatal closure. These effects were phenocopied with rotenone, which increased mitochondrial ROS. In contrast, the mitochondrially targeted antioxidant, MitoQ, dampened ABA effects on mitochondrial ROS accumulation and stomatal closure in Col-0 and reversed the guard cell closure phenotype of the *abo6* mutant. ABA-induced ROS accumulation in guard cell mitochondria was lost in mutants in genes encoding respiratory burst oxidase homolog (RBOH) enzymes and reduced by treatment with the RBOH inhibitor, VAS2870, consistent with RBOH machinery acting in ABA-increased ROS in guard cell mitochondria. These results demonstrate that ABA elevates $H_2O_2$ accumulation in guard cell mitochondria to promote stomatal closure.

## Introduction

Drought stress negatively impacts plant growth due to excess water loss, which is a growing concern for crop yields as a result of the changing global climate (Fahad et al., 2017). Stomatal closure reduces excess water loss but also limits $CO_2$ entry, thereby negatively impacting the photosynthetic rate (Lamaoui et al., 2018). Due to this tradeoff, stomatal aperture must be tightly controlled (Nilson and Assmann, 2007). Reduction in guard cell turgor to close stomata is mediated by the hormone abscisic acid (ABA), which signals in guard cells during states of decreased water availability (Xu et al., 2016, Li et al., 2017, Qi et al., 2018, Qu et al., 2018, Tõldsepp et al., 2018).

The binding of ABA to the pyrabactin resistance1/PYR1-like/regulatory components of ABA receptor (PYR/PYL/RCAR) family of soluble receptors initiates an ABA signaling cascade (Park et al., 2009). The ABA-bound receptors form a complex with Clade A protein phosphatases type 2C (PP2Cs), which negatively regulate ABA signaling in the absence of the

Received August 30, 2022. Accepted December 4, 2022. Advance access publication December 27, 2022

hormone (Hsu et al., 2021). Formation of this complex inhibits PP2C activity, releasing the negative regulation of the pathway (Ma et al., 2009, Park et al., 2009, Nishimura et al., 2010). Reduced phosphatase activity allows for increased phosphorylation of a variety of proteins including Sucrose nonfermenting Related Kinase 2 family members (SnRK2s) (Takahashi et al., 2020). Active SnRK2s can then further promote the signaling cascade through phosphorylation of a number of downstream targets including Respiratory Burst Oxidase Homologs (RBOH) enzymes, also called NADPH-oxidase (NOX) enzymes (Sirichandra et al., 2009). Consistent with RBOH activation, reactive oxygen species (ROS) accumulation in guard cells following ABA treatment has been observed in multiple plant species (Pei et al., 2000, Kwak et al., 2003, Watkins et al., 2014, 2017). These elevated ROS act as second messengers that lead to decreases in $H^+$ export and $K^+$ uptake, while increasing the efflux of $K^+$, $Cl^-$, and malate. This results in the reduction of guard cell turgor and closure of the stomatal pore (Geiger et al., 2009, Demidchik, 2018, Jezek and Blatt, 2017, Klejchova et al., 2021).

ROS bursts resulting from RBOH activation have been characterized in plants in response to a myriad of developmental and environmental signals (Chapman et al., 2019, Martin et al., 2022). These enzymes function in the production of extracellular superoxide through the transfer of electrons from NADPH or $FADH_2$ to molecular oxygen (Suzuki et al., 2011). Superoxide may be rapidly converted to $H_2O_2$ spontaneously or by enzymatic means via superoxide dismutases (Fukai and Ushio-Fukai, 2011). Extracellular $H_2O_2$ may then enter plant cells through plasma membrane-localized aquaporins (Bienert et al., 2007, Tian et al., 2016, Rodrigues et al., 2017). The Arabidopsis (*Arabidopsis thaliana*) genome encodes 10 RBOH family members (RBOHA–RBOHJ) with distinct expression patterns and functions that regulate a variety of developmental and cellular processes (Chapman et al., 2019). Genetic approaches have identified a role for RBOHF during ABA-induced stomatal closure (Kwak et al., 2003). Both the *rbohf* single mutant and the *rbohd/f* double mutant displayed a reduction in both ABA-driven ROS increases and stomatal closure when compared with wild-type guard cells (Kwak et al., 2003).

Insight into the subcellular location where ROS accumulates in guard cells after ABA treatment, as well as the type of ROS that is increased, is needed to fully understand how these molecules function in ABA signaling. Prior studies examining ABA-dependent increases in ROS accumulation have largely examined changes in fluorescence of dichlorofluorescein (DCF), the cleavage product of chloromethyl 2,7-dihydrodichlorofluorescein diacetate (CM $H_2$DCF-DA), a cell-permeable generic ROS sensor (Pei et al., 2000, Kwak et al., 2003, Zhang et al., 2001, Wu et al., 2017, An et al., 2016), which does not reveal which types of ROS are increased by ABA (Winterbourn, 2014, Kalyanaraman et al., 2012). Prior work has shown that the transcriptional responses downstream from ROS signals appear to hold a level of specificity based not only on what type of ROS is being sensed but also on where a given ROS is being generated (Gadjev et al., 2006). While redox changes in plants have been characterized in response to a myriad of environmental responses in multiple tissues, studies providing details on the type of ROS produced and where the ROS are accumulating are sparse. Therefore, there are still many questions remaining that require ROS detection methodology that can allow visualization of specific types of ROS in a particular subcellular compartment. While this is a difficult task given the highly reactive nature of these molecules, excellent advancements have been made in both microscopic resolution and ROS detection using chemical or genetically encoded sensors, with the roGFP2-Orp1 bioreporter providing substantial insight into the localization of hydrogen peroxide (Nietzel et al., 2019, Winterbourn, 2014, Ugalde et al., 2021b, Dickinson et al., 2010). Together, these tools have provided the ability to gain better insight into this spatial accumulation of different ROS species in response to environmental stresses, hormone signaling, and development.

This study examined how ABA affects the accumulation and localization of $H_2O_2$ within Arabidopsis guard cells during the ABA response and how each of these intracellular compartments contribute to total ROS changes that drive stomatal closure. The subcellular distribution of the general ROS sensor, DCF, was examined across multiple subcellular locations including the guard cell chloroplasts, cytosol, nuclei, and cytosolic puncta that we identified as mitochondria. To verify that the compartmentalized ROS changes were directly tied to ABA signaling, we examined these ROS changes in the ABA quintuple receptor mutant (*pyl-11458*). To determine if $H_2O_2$ increases in response to ABA, both Peroxy Orange 1, a chemical probe selective for $H_2O_2$, and the roGFP2-Orp1 genetically encoded hydrogen peroxide sensor, which was targeted to the cytosol, mitochondria, or chloroplast, were used to provide insight into changes in this signaling ROS. Genetic and pharmacological approaches were also used to manipulate mitochondrial ROS production to test the role of this localized ROS in ABA-dependent stomatal closure. This combination of chemical, genetic, and imaging approaches reveals that ABA increases $H_2O_2$ in guard cell mitochondria and that ROS increases within this organelle play a necessary role in ABA-induced stomatal closure.

## Results

### ABA signaling drives compartmentalized ROS increases within guard cells

ABA-induced ROS increases within Arabidopsis guard cells were verified through quantification of fluorescence intensity changes using a generic ROS-responsive fluorescent probe. We utilized chloromethyl 2,7-dihydrodichlorofluorescein diacetate (CM $H_2$DCF-DA), which is a frequently utilized fluorescent chemical probe to monitor changes in ROS accumulation (Halliwell and Whiteman, 2004). CM $H_2$DCF-DA diffuses across the plasma membrane, where it is trapped

within the cell after cleavage by cellular esterases (Swanson et al., 2011). The probe is then converted to the highly fluorescent DCF upon oxidation by ROS. Whole leaves of Col-0 were excised in the morning, epidermal peels were prepared and then covered with a stomatal opening solution for 3 h under white light to fully open stomata. This was followed by incubation with 20 μM ABA or a control treatment for 45 min. Treatments were then removed, and leaf peels were incubated with CM $H_2$DCF-DA for 15 min. Laser scanning confocal microscope (LSCM) images of guard cells with control or ABA treatment with the images of DCF fluorescence are shown directly and after conversion to lookup tables (LUT), which clarifies the range of fluorescence across these cells, with representative images shown in Supplemental Figure 1A. Whole stomata DCF fluorescence was recorded in 30 or more stomata per treatment and each individual value was normalized relative to the average signal intensity of control buffer-treated stomata. This quantification confirmed that ABA significantly increased DCF fluorescence in guard cells during ABA-induced stomatal closure (Supplemental Figure 1B).

The images in Supplemental Figure 1 suggest that ABA increases the DCF signal in a number of distinct subcellular locations. We therefore performed high-resolution imaging of Col-0 guard cells in the presence and absence of 20 μM ABA for 45 min to identify the location within the cell that ABA signaling increased ROS. ABA treatment increased DCF fluorescence within multiple subcellular regions (Figure 1). The DCF signal increases in the chloroplast and nucleus were verified through spectral unmixing of the DCF signal from chlorophyll autofluorescence and 4′,6-diamidino-2-phenylindole fluorescence, respectively (Supplemental Figure 2A–B). DCF fluorescence is largely excluded from the vacuole, but there are increases in DCF signal after ABA treatment in the chloroplasts, cytosol, nucleus, and small cytosolic punctate structures (Figure 1A), which we identified as mitochondria in experiments described below. To determine how each of these subcellular regions contributes to overall ROS changes, we quantified increases in each of these locations. Following 45 min of 20 μM ABA treatment, we observed the largest increases within the mitochondria and chloroplasts at 1.5-fold and 1.8-fold, respectively, when compared with control-treated guard cells (Figure 1, B and C). We also observed significant increases in other locations with a 1.3-fold ABA-induced increase within guard cell nuclei (Figure 1D) and a 1.4-fold increase in the cytosolic signal (Figure 1E).

To determine whether these subcellularly localized ABA-induced ROS changes were downstream of the canonical ABA signaling pathway, we also examined the response in the ABA quintuple receptor mutant (*pyl-11458*). The DCF fluorescence in the mitochondria, nucleus, and cytoplasm was no longer significantly different between control buffer and ABA treatment in the *pyl-11458* mutant (Antoni et al., 2013). In the chloroplasts, the magnitude of the ABA-dependent increase was reduced relative to Col-0, although there was still a significant difference in response to ABA treatment (Figure 1, B–E). These data suggest that ABA increased ROS in several intracellular locations within guard cells; however, DCF cannot resolve which ROS increases.

## ABA increases $H_2O_2$ in subcellular regions including chloroplasts and mitochondria to induce stomatal closure

To ask whether hydrogen peroxide ($H_2O_2$) is the ROS that increases in response to ABA, we utilized the $H_2O_2$-selective chemical probe, Peroxy Orange 1 (PO1) (Dickinson et al., 2010), which is a membrane-permeable, boronate-based probe that becomes fluorescent upon irreversible oxidation by $H_2O_2$. The spectral profile of PO1 was isolated and unmixed from leaf autofluorescence, including chloroplasts, and the signal in the absence and presence of ABA is shown in Figure 2A. Treatment with 20 μM ABA significantly increased the PO1 signal in the chloroplasts but did not result in a significant increase in the mitochondria (Figure 2, B and C), nucleus, or cytosol (Supplemental Figure 3). To determine if higher concentrations of ABA were sufficient to stimulate $H_2O_2$ increases throughout guard cells, we increased the concentration of ABA to 100 μM.

Following treatment with 100 μM ABA, we observed a small but significant increase in PO1 signal within mitochondria (Figure 2B) as well as a significant increase in PO1 signal in chloroplasts (Figure 2C). However, the PO1 signal in the cytosol and nucleus was once again not significantly different from control treatments (Supplemental Figure 3C–D). This suggests that PO1 may not be taken up by all organelles or that PO1 may not be sensitive enough to detect the $H_2O_2$ changes displayed in certain subcellular locations.

To verify that PO1 fluorescence is ROS responsive in the nucleus, we treated guard cells with 250 μM exogenous $H_2O_2$ (Supplemental Figure 4A–C). Treatment with exogenous $H_2O_2$ resulted in a 1.5-fold increase in nuclear PO1 fluorescence, indicating that PO1 can be sufficiently taken up by Arabidopsis guard cell nuclei to detect large increases in $H_2O_2$ (Supplemental Figure 4C). The effect of this exogenous $H_2O_2$ treatment on stomatal closure was quantified in Supplemental Figure 4B. Treatment with exogenous $H_2O_2$ for 30 min was sufficient to close stomata to levels consistent with ABA-dependent closure. Together, these results suggest that $H_2O_2$ can function as the ROS to close stomata, but that ABA-induced increases in $H_2O_2$ in guard cells may need more sensitive tools than PO1 for their detection.

In the chloroplast, we observed ABA-induced PO1 accumulation into distinct structures within inner chloroplast compartments. However, 2D images of maximum intensity projection make it difficult to discern if these dyes are associated with the chloroplast membrane or internal to this organelle. Therefore, we created 3D renderings of PO1-labeled guard cells to gain insight into chloroplast PO1 distribution (Supplemental Figure 5).

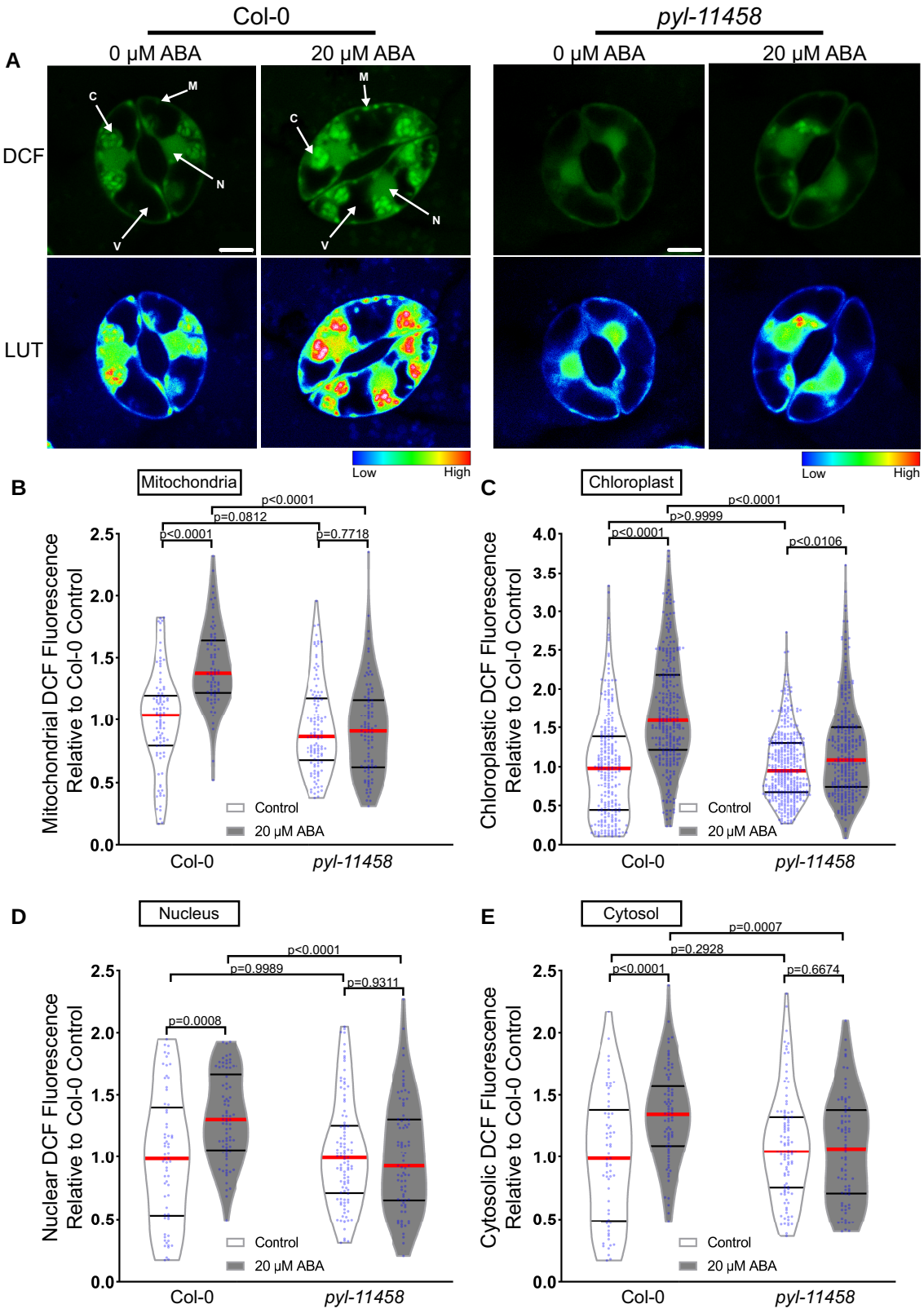


**Figure 1** ABA treatment increases dichlorofluorescein (DCF) fluorescence in multiple subcellular locations within Arabidopsis guard cells. A, Confocal micrographs of DCF fluorescence of guard cells in leaves from Col-0 or a quintuple ABA receptor mutant, *pyl-11458*, treated with control buffer or 20 μM ABA shown directly or after conversion to LUT. Subcellular compartments are indicated on each image (C, Chloroplast; N, Nucleus; M, Mitochondria; V, Vacuole). Scale bar: 5 μm. Quantifications of DCF fluorescence in the (B) mitochondria, (C) chloroplasts, (D) nucleus, and (E) cytosol with and without ABA treatment from three separate experiments (chloroplast $n > 100$, nucleus $n > 48$, cytosol $n > 48$, and mitochondria $n > 56$). All individual values were normalized to the average of the control treatment for Col-0 in each subcellular location and are displayed on the graph as blue dots with the median shown in red and lower and upper quartiles indicated in black. All *P*-values were calculated by two-way ANOVA followed by a Tukey's post hoc test from at least three separate experiments.

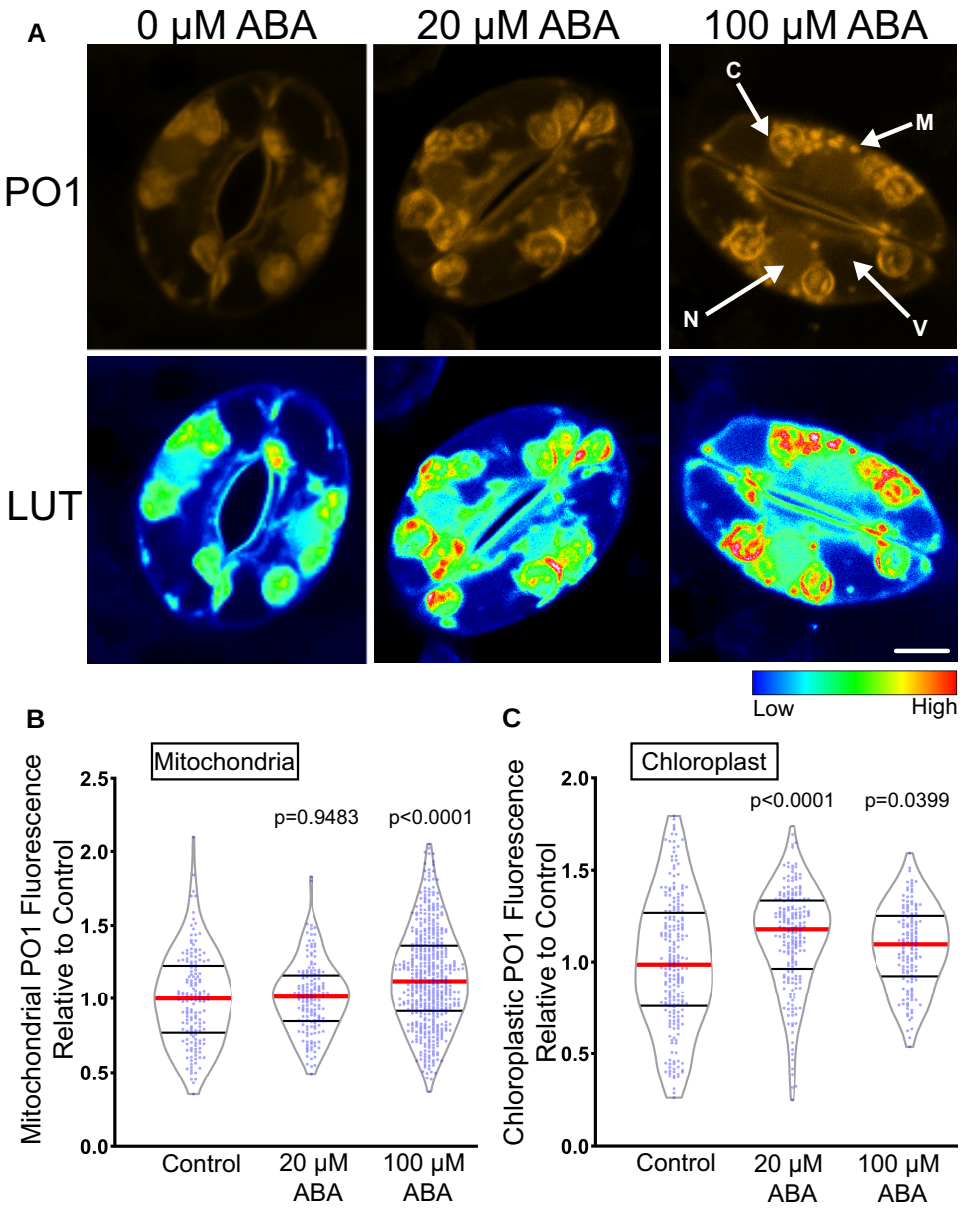


**Figure 2** ABA increases fluorescence of Peroxy Orange 1 (PO1), a hydrogen peroxide selective dye. A, Confocal micrographs of PO1 fluorescence or PO1 signal converted to lookup tables (LUT) after treatment with 0, 20, or 100 μM ABA. Maximum intensity projections of full z-stacks are shown. Scale bar: 5 μm. Quantifications of PO1 fluorescence in (B) mitochondria and (C) chloroplasts. All individual values were normalized to the average of the control treatment for each subcellular location and are displayed on the graph as blue dots with the median shown in red and lower and upper quartiles indicated in black. All *P*-values were calculated by one-way ANOVA followed by a Tukey's post hoc test from at least three separate experiments (mitochondria $n > 148$ and chloroplast $n > 140$).

These renderings show that bright PO1 regions span the chloroplast and are not just on the surface, revealing a complex ROS accumulation pattern within the chloroplast. The PO1 localized signal is similar in position and size to the accumulation of starch grains (Leshem and Levine, 2013), though we cannot currently rule out that the complex accumulation pattern of PO1 fluorescence in chloroplasts is due to increased dye sequestration in regions within this organelle. In contrast, the mitochondria are circular structures with uniform PO1 signal.

## ABA treatment results in DCF increases within guard cell mitochondria

DCF and PO1 localized to small cytosolic punctate structures in addition to chloroplasts and nuclei. We used colocalization of chemical ROS probes with fluorescent organelle dyes and an organelle-targeted green fluorescent protein (GFP) to ask whether these puncta are ROS-producing peroxisomes or mitochondria (Figure 3). To evaluate whether cytosolic ROS puncta were peroxisomes, we examined an Arabidopsis transgenic line with a GFP

tagged with a type 1 peroxisomal targeting signal (GFP-PTS1) (Ramón and Bartel, 2010) (Figure 3A). GFP-PTS1 and PO1 have emission peaks that can be spectrally unmixed. We used the Zen colocalization module to draw ROIs around cytosolic punctate structures that did not overlay on a chloroplast (Figure 3B). Although the GFP-PTS1 signal accumulated into punctate structures within the guard cell cytosol, they did not colocalize with the puncta labeled with PO1 (Figure 3C).

To determine whether these puncta colocalize with mitochondria, we labeled Col-0 guard cells with Mitotracker Red prior to staining with CM $H_2$DCF-DA. Figure 3D shows Mitotracker (magenta), DCF signal (green), and chlorophyll signal (red), separately and in an overlay. All of the DCF puncta contained Mitotracker red signal. We drew ROIs around more than 40 DCF puncta (Figure 3E). Also, these structures display higher DCF intensity than most other localizations which allowed us to use the lowest intensity puncta to define the colocalization threshold and generate a colocalization graph (Figure 3F). A majority of pixels in the designated ROIs contain both DCF and Mitotracker Red signals, and we calculated the average weighted colocalization coefficient to be 0.96. These results are consistent with the punctate structures showing ABA-dependent ROS changes being mitochondria.

## Genetically encoded ROS biosensor roGFP2-Orp1 showed rapid ABA-dependent $H_2O_2$ increases within guard cell nuclei and cytosol

Although chemical ROS probes have provided us with a framework to identify subcellular locations in which ABA drives ROS increases in guard cells, these sensors suffer from disadvantages such as irreversibility and differential dye uptake into some subcellular compartments (Martin et al., 2022). Thus, more precise tools are necessary to reliably evaluate ABA-dependent oxidation in guard cells. Therefore, we evaluated changes in $H_2O_2$ using the genetically encoded biosensor, roGFP2-Orp1, which has enhanced sensitivity relative to PO1, can be targeted to different subcellular locations and provides a ratiometric readout that is not affected by changes in pH (Nietzel et al., 2019). In the presence of $H_2O_2$, the yeast peroxidase Orp1 (also known as glutathione peroxidase 3) becomes oxidized to sulfenic acid (Cys-SOH) on a reactive cysteine residue that rapidly forms an intramolecular disulfide bond with a nearby cysteine. This disulfide is then efficiently transferred via thiol–disulfide exchange to a pair of cysteines on roGFP2, resulting in a conformational change that alters the optical properties of the fluorophore (Gutscher et al., 2009). When reduced, the sensor has increased signal intensity after excitation with the 488 nm laser line, while oxidation leads to elevated signal following 405 nm excitation. Therefore, dividing signal intensity after 405 nm excitation by intensity following 488 nm excitation provides a ratiometric readout that has an internal control for expression levels within a particular tissue (Nietzel et al., 2019).

To identify the dynamic range of this sensor in guard cells, we treated guard cells with 20 mM dithiothreitol (DTT) to reduce this biosensor, which leads to a low 405/488 fluorescence ratio (Supplemental Figure 6). In contrast, treatment with 10 mM $H_2O_2$ increases protein oxidation leading to an elevated 405/488 fluorescence ratio. To examine the effect of ABA on the oxidation of this sensor, we excised fully mature Arabidopsis leaves containing roGFP2-Orp1 and generated epidermal leaf peels as described earlier (Figure 4). The process of generating an epidermal leaf peel is mechanical stress, which can increase roGFP2-Orp1 oxidation (Scuffi et al., 2018). We verified that incubation of the epidermal leaf peels in the stomatal opening buffer for 4 h prior to any treatment allowed oxidation to begin returning to baseline levels. Stomatal opening buffer was removed following equilibration and replaced with a similar solution containing 20 μM ABA or control treatment for 45 min. Figure 4A shows the fluorescence of roGFP2-Orp1 guard cells excited at either 405 or 488 nm and illustrates that, consistent with oxidation of this reporter after ABA treatment, the fluorescence of a sample excited at 405 nm is elevated and the fluorescence of the sample excited at 488 nm is reduced. The increase in oxidation after ABA treatment is most evident when the ratio of fluorescence is illustrated as a heat map, with this being generated by a MatLab program (Fricker, 2016) (Figure 4A). We quantified the effect of ABA treatment in roGFP2-Orp1 oxidation in whole stomata, which resulted in a 1.4-fold increase in oxidation ratio when compared with control guard cells (Figure 4B). The dynamic range of the sensor as judged by DTT and $H_2O_2$ treatment defining the minimum and maximum is noted on the graph in Figure 4, B–E. These data are consistent with ABA driving an increase in guard cell $H_2O_2$ during stomatal closure.

A potential benefit of using this genetically encoded sensor is the ability to monitor changes in $H_2O_2$ within individual guard cells over time to gain insights into the spatial dynamics of ABA-dependent increases in $H_2O_2$. The changing sensor oxidation over time in these guard cells treated with ABA and then treated with DTT to reverse this oxidation is shown in Supplemental Figure 7A. The challenge of continuous illumination of the same guard cells is that it can lead to light-induced oxidation of the sensor due to the excitation of chloroplasts leading to increases in $H_2O_2$ (Ugalde et al., 2021a). Consistent with this prior report, we can initially detect differences in sensor oxidation between ABA-treated and buffer control samples, but after 30 min of imaging, the amount of oxidation of the sensor in the control became similar to the ABA-induced oxidation (Supplemental Figure 7B). Therefore, rather than time course imaging, we minimized the effect of light on sensor oxidation by imaging multiple different samples at several time points as we did previously with chemical probes.

To examine the temporal dynamics of $H_2O_2$ accumulation within the cytosol and nucleus following ABA treatment, we monitored shifts in oxidation ratio within guard cells transformed with roGFP2-Orp1 by drawing ROIs in these

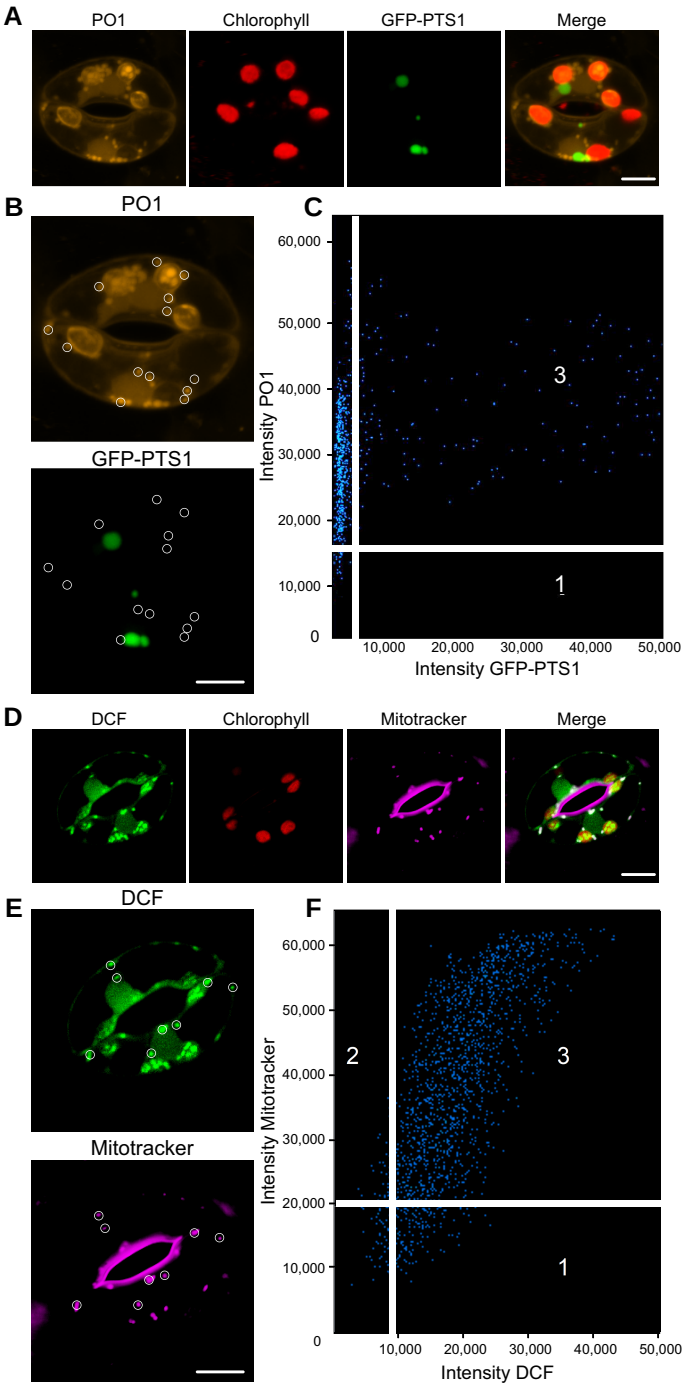


**Figure 3** ABA treatment results in increased ROS accumulation in cytosolic puncta that colocalize with mitochondria. A, Confocal micrographs of Peroxy Orange 1 (PO1) fluorescence (orange), chlorophyll autofluorescence (red), GFP-PTS1 (peroxisomal targeting signal 1) (green), and a merged image. Maximum intensity projection of full z-stack is shown. B, Regions of interest used to generate a weighted colocalization coefficient are circled in white, highlighting the absence of PO1 fluorescence colocalizing with GFP-PTS1 fluorescence. C, Colocalization graph generated with the ZEN Black colocalization module from regions of interest highlighting PO1-labeled cytosolic puncta. Numbers on the scatterplot represent data points that either fall below the determined intensity cutoff for PO1 (1) or GFP-PTS1 (2), or data points that are above thresholding limits for both fluorescent reporters (3). D, Confocal micrographs of dichlorofluorescein (DCF) fluorescence (green), chlorophyll autofluorescence (red), Mitotracker (magenta), and a merged image showing DCF colocalized with Mitotracker (white). E, Regions of interest used to generate a weighted colocalization coefficient are circled in white, showing DCF fluorescence colocalizing with Mitotracker fluorescence. F, Colocalization graph generated with the ZEN Black colocalization module from regions of interest highlighting DCF-labeled cytosolic puncta. Numbers on scatterplot represent data points that either fall below the determined intensity cutoff for Mitotracker (1) or DCF (2), or data points that are above thresholding limits for both fluorescent reporters (3). Scale bars: 5 μm.

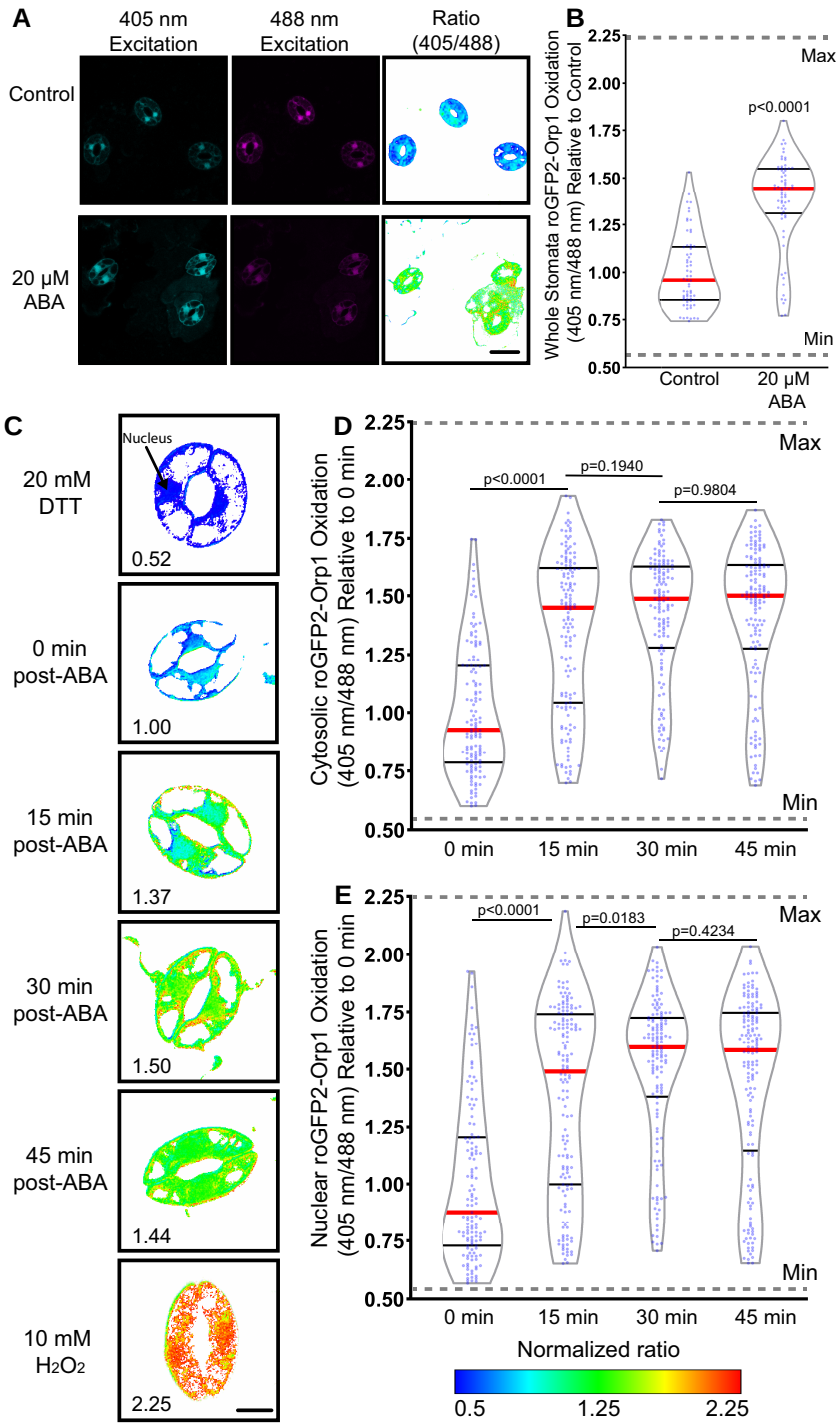


**Figure 4** roGFP2-Orp1 detects ABA-increased hydrogen peroxide ($H_2O_2$) within the guard cell cytosol and nuclei. A, Confocal micrographs of Arabidopsis guard cells expressing roGFP2-Orp1 treated with 20 µM ABA for 45 min after excitation with either 405 or 488 nm laser line are shown along with ratiometric images that display fluorescence ratios calculated from those images. Scale bar: 20 µm. B, Quantification of intracellular roGFP2-Orp1 ratios following 20 µM ABA or control treatment. Ratios are the fluorescence intensity collected after excitation at 405 nm divided by the intensity after 488 nm excitation. All individual values were normalized to the average of the control treatment and are displayed on the graph as blue dots with the median shown in red and lower and upper quartiles indicated in black with data from three separate experiments ($n = 64–69$) whole stomata for each treatment). *P*-values were calculated from Student's *t*-tests. C, Confocal micrographs of Arabidopsis guard cells converted to ratiometric values from cells expressing roGFP2-Orp1 treated with 20 µM ABA for 0, 15, 30, or 45 min. Minimum and maximum sensor oxidation are shown by treatment with 20 mM dithiothreitol (DTT) or 10 mM $H_2O_2$, respectively. Ratios are calculated as above. Normalized ratios are then created relative to the average for the 0 min timepoint. D, Quantification of roGFP2-Orp1 ratio in the cytosol and (E) nucleus following 20 µM ABA for 0, 15, 30, or 45 min. Data are reported from three separate experiments ($n > 131$ guard cells for each time point). Minimum and maximum sensor oxidation is represented on graphs by gray dashed lines. The significance of differences between indicated time points was determined by one-way ANOVA followed by Tukey's multiple comparisons tests and are shown on the graph. Scale bar: 5 µm.

locations. Although this roGFP2-Orp1 protein fusion is targeted to the cytosol, the biosensor also shows a signal in the guard cell nucleus (Babbar et al., 2021, Nietzel et al., 2019), allowing us to also monitor $H_2O_2$ changes in this organelle. Leaves expressing roGFP2-Orp1 were peeled and equilibrated in stomatal opening solution as described earlier. The opening buffer was then removed following equilibration and replaced with 20 μM ABA for 0, 15, 30, or 45 min (Figure 4C). Though roGFP2-Orp1 was still slightly oxidized in both the cytosol and nucleus after 4 h incubation in stomatal opening solution, treatment with 20 μM ABA resulted in a significant increase in oxidation above baseline in both locations within 15 min (Figure 4, D and E). ABA treatment led to continued oxidation of the sensor in a time-dependent manner, reaching a maximum of 1.4-fold increase over control in the cytosol and 1.5-fold in the nucleus at 30 min with the oxidation ratio beginning to decrease at 45 min (Figure 4, C–E).

## ABA treatment increases the oxidation of roGFP2-Orp1 targeted to the mitochondria and chloroplast

To confirm that ABA perception drives $H_2O_2$ accumulation in guard cell mitochondria, we examined a transgenic line expressing roGFP2-Orp1 specifically in the mitochondrial matrix (mt-roGFP2-Orp1) (Nietzel et al., 2019) (Figure 5). To minimize oxidation due to the generation of the leaf peel, we equilibrated samples in a stomatal opening solution for 4 hours before imaging. We determined the dynamic range of this reporter using DTT to fully reduce the reporter and $H_2O_2$ to fully oxidize it, as shown in Supplemental Figure 8 and Figure 5B. It is evident that the signal of this reporter is dispersed in puncta throughout the cytosol, which is most evident in the $H_2O_2$-treated samples. Since the emission spectra of GFP following excitation with its optimal wavelength (488 nm) are easily unmixed from that of PO1 emission at the same excitation wavelength, we utilized this sensor to verify that PO1-labeled puncta were also identified as mitochondria through colocalization of these two signals (Supplemental Figure 9).

Treatment with 20 μM ABA resulted in a significant increase in oxidation signal of this mitochondrial sensor at 45 min after ABA treatment (Figure 5B). It is of note that the mt-roGFP2-Orp1 oxidation state across the entire mitochondrial population is less uniform than with the sensor targeted to the cytoplasm (Figure 4C). This may be responsible for the lower magnitude change in response to ABA in mt-roGFP2-Orp1 when compared with the ABA increase the mitochondrial signal of chemical ROS probes.

We also examined the effect of ABA on roGFP2-Orp1 targeted to the chloroplast (plastid-roGFP2-Orp1) (Ugalde et al., 2021a). We did detect a significant increase in sensor activity, supporting our result with chemical sensors (Supplemental Figure 10). However, ABA induced a lower magnitude response in this reporter than seen via DCF, suggesting another ROS type or disproportionate localization of the chemical probe to this organelle. The magnitude of the ABA changes in these two sensors in the mitochondria and chloroplasts cannot be directly compared because of multiple technical differences, but in both organelles we see ABA responses mirroring that seen with chemical reporters of ROS changes. Altogether, we used a sophisticated biosensor to demonstrate that ABA increases $H_2O_2$ with similar spatial and temporal responses to ROS changes detected with chemical sensors, strengthening the evidence for ROS as second messengers in ABA-dependent stomatal closure.

## Mutations or treatments that alter mitochondrial ROS accumulation influence ABA-dependent stomatal closure

To evaluate the function of ABA-induced ROS in guard cell mitochondria, we searched for mutants with altered ABA response tied to mitochondrial function. *ABA overly sensitive 6* (*abo6*) was identified in a genetic screen evaluating the ability of ABA to inhibit primary root elongation (He et al., 2012). Consistent with an enhanced response to ABA, this mutant displayed drought tolerance (He et al., 2012). The *abo6* mutation maps to a gene encoding a mitochondrial DEXH (Asp-Glu-x-His) box RNA helicase that functions in the splicing of several transcripts that are required for the proper function of complex I in the mitochondrial electron transport chain and the protein product of this gene is only expressed in mitochondria (He et al., 2012). Because complex I is a major source of ROS production, impairment at this site can result in increased electron leakage and thus elevated mitochondrial ROS. To ask whether the *abo6* mutant was also enhanced in ABA response in guard cells, we examined the levels of DCF fluorescence in the mitochondria in guard cells of *abo6* (Figure 6A). We found that *abo6* contained 1.3-fold higher levels of DCF fluorescence in guard cell mitochondria when compared with Col-0 under control conditions. Additionally, ABA treatment yielded a 1.2-fold higher DCF signal in the *abo6* mutant background than in Col-0 and had a larger ABA response when compared with its untreated control than Col-0 (Figure 6B). These results demonstrate that *abo6* has an enhanced ABA response in guard cells, consistent with the elevated root ABA responses.

To examine the effect of mitochondrial ROS on guard cell ABA sensitivity, we examined ABA-induced stomatal closure in *abo6* guard cells and in Col-0 guard cells with pharmacological perturbations of mitochondrial ROS (Figure 6C). Here, we utilized rotenone, an inhibitor of complex I in the mitochondrial electron transport chain (Palmer et al., 1968) that can result in increased electron leakage out of complex I and ultimately increased accumulation of mitochondrial ROS (Mohammed et al., 2020, Li et al., 2003, Zhou et al., 2014). We also used the mitochondrially targeted antioxidant MitoQ (Kelso et al., 2001), to determine its effect on ABA-increased oxidation of mt-roGFP2-Orp1. We treated guard cells with 500 nM MitoQ in advance of ABA treatment. This treatment

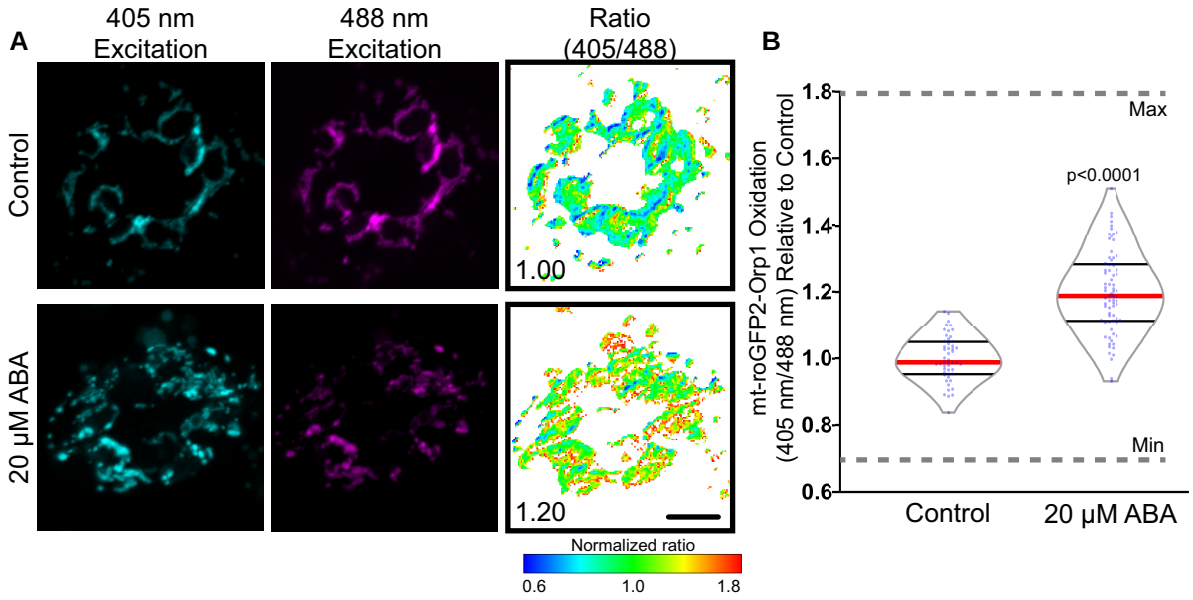


**Figure 5** Mitochondrially targeted roGFP2-Orp1 reveals ABA-dependent hydrogen peroxide ($H_2O_2$) increases. A, Confocal micrographs of Arabidopsis guard cells expressing mt-roGFP2-Orp1 treated with 20 μM ABA or control buffer for 45 min. Ratiometric images display fluorescence ratios calculated from separate images taken using sequential excitation at 488 and 405 nm for each time point. Ratios are calculated by dividing fluorescence intensity collected at emission window 500–535 nm after excitation at 405 nm by the intensity collected in the same emission window after 488 nm excitation. Scale bar: 5 μm. B, Quantification of mt-roGFP2-Orp1 ratio in the entire guard cell following 20 μM ABA or buffer control for 45 min. All individual values were normalized to the average of the control treatment and are displayed on the graph as blue dots with the median shown in red and lower and upper quartiles indicated in black. Minimum and maximum sensor oxidation are shown by treatment with 20 mM dithiothreitol (DTT) or 10 mM $H_2O_2$, respectively. Data are reported from three separate experiments ($n > 50$ stomata). Minimum and maximum sensor oxidation, determined by treatment with DTT and $H_2O_2$, respectively, is represented on graphs by gray dashed lines. Listed *P*-values were determined by one-way ANOVA followed by Tukey's post hoc tests. Scale bars: 5 μm.

abolished the ABA-induced increase in mt-roGFP2-Orp1 fluorescence (Figure 6D). We were unable to find reports of this inhibitor being used in plants, suggesting that its specificity toward mitochondria in photosynthetic organisms has not been adequately tested. MitoQ has structural similarity with plastoquinone found in the chloroplast, so we examined MitoQ's effect on ABA-dependent oxidation of plastid-roGFP2-Orp1. MitoQ lead to a reduction in the oxidation of chloroplast plastid-roGFP2-Orp1 sensor when compared with the ABA-only treatment, but not to levels of untreated leaves (Supplemental Figure 11). This MitoQ effect was substantially smaller than the effect on the mitochondrial sensor, which completely reversed the effect of ABA resulting in levels of sensor oxidation that were lower than in the absence of ABA treatment (Figure 6D).

To evaluate the effect of Mito Q on stomatal closure, leaves were excised and peeled and then pretreated with either stomatal opening buffer as described previously, 500 nM MitoQ for 3 h, or 50 μM rotenone for 1 h. Epidermal peels were then treated with 20 μM ABA for 0, 15, 30, or 45 min, and guard cells were immediately imaged (Figure 6C). Initial apertures after incubation in an opening solution showed a slight difference between Col-0 and *abo6* prior to any ABA treatment, consistent with the elevated levels of baseline mitochondrial ROS observed in Figure 6B. Following 20 μM ABA treatment, *abo6* showed a significant increase in ABA-dependent closure relative to Col-0. Unlike *abo6*, rotenone pretreatment alone did not significantly alter initial stomatal aperture measurements prior to treatment with ABA. However, rotenone pretreatment significantly increased the amount of stomatal closure over the 45-min time course of ABA treatment. We also examined the effect of pretreatment with MitoQ on stomatal closure, finding that it significantly reduced ABA-dependent stomatal closure in Col-0 and was able to rescue the hypersensitive ABA response in *abo6* guard cells so that the stomatal aperture was not significantly different from that of Col-0 (Figure 6E). These findings are consistent with ABA driving ROS increases in guard cell mitochondria and indicate that the degree of ABA sensitivity is associated with the amount of ROS production within this organelle.

## Mutants deficient in *rbohd* and *rbohf* have impaired ABA-induced ROS accumulation in several subcellular locations

RBOH enzymes are well-characterized producers of signaling ROS that regulate a myriad of plant developmental processes and environmental responses (Chapman et al., 2019). To determine whether RBOH enzymes are linked to the increase in ROS accumulation in mitochondria following ABA treatment, we examined DCF fluorescence in Arabidopsis mutants with defects in the genes encoding RBOHD and

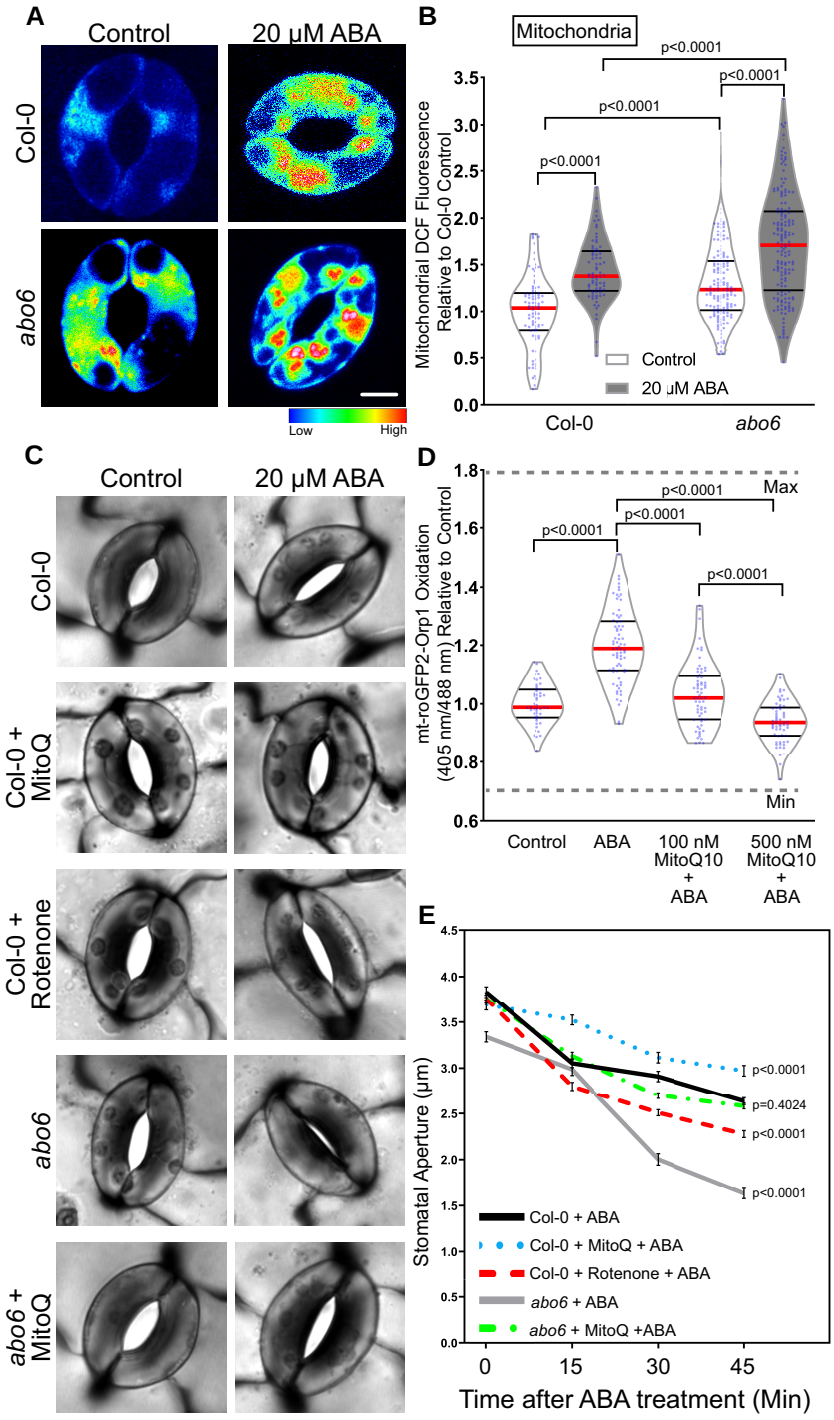


**Figure 6** Perturbations in mitochondrial reactive oxygen species influence the rate of ABA-induced stomatal closure. A, Confocal micrographs of dichlorofluorescein (DCF) fluorescence following conversion to LUT for *ABA overly sensitive* (*abo6*) guard cells treated with control buffer or 20 μM ABA for 45 min. Scale bar: 5 μm. B, DCF fluorescence was quantified within mitochondria of Col-0 and *abo6* guard cells with and without ABA treatment from three separate experiments and is reported relative to untreated Col-0, with each bar represented by ($n > 75$) guard cells. C, Stomatal apertures of leaves of Col-0 or *abo6* pretreated with either control buffer, 50 μM rotenone for 1 h or 500 nM MitoQ for 3 h and then treated with 20 μM ABA for 45 min. Scale bar: 5 μm. D, Quantification of mt-roGFP2-Orp1 ratio of the entire guard cell following 20 μM ABA, buffer control, or pretreatment with either 100 or 500 nM MitoQ for 3 h followed by ABA treatment for 45 min ($n = 65$). E, Stomatal apertures of Col-0 and *abo6* leaves were quantified at 0, 15, 30, and 45 min after ABA treatment ($n > 85$ stomata/per reported value) in the presence and absence of MitoQ or rotenone, with the average and standard error of the mean graphed at each time point. All individual values in (B) and (D) were normalized to the average of the control treatment for Col-0 and are displayed on the graph as blue dots with the median shown in red and lower and upper quartiles indicated in black. The *P*-values for each quantification were generated by two-way ANOVA of the entire time course for each genotype/treatment, followed by Tukey's post hoc tests.

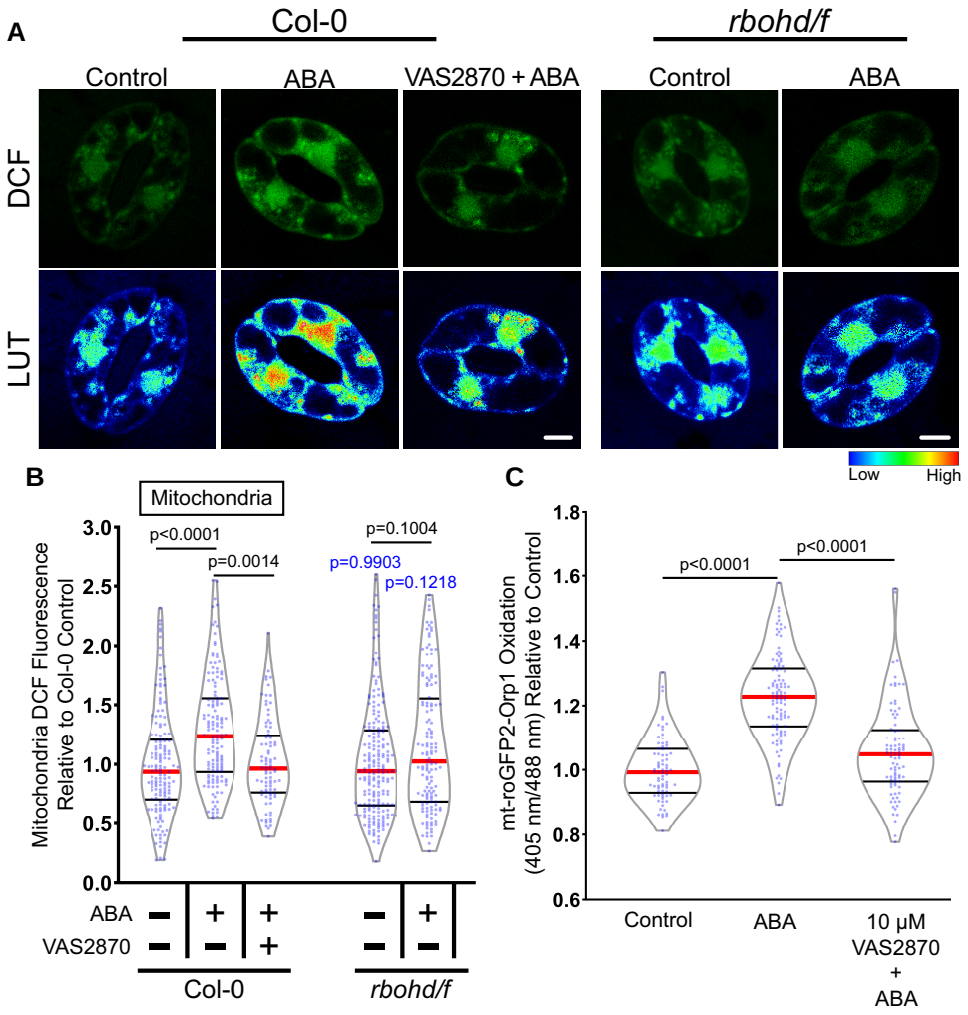


**Figure 7** Respiratory burst oxidase homologs (RBOH) enzymes contribute to ABA-increased ROS accumulation in guard cell mitochondria. A, Confocal micrographs of dichlorofluorescein (DCF) fluorescence or DCF images converted to a lookup table (LUT) of Col-0 or *rbohd/f* guard cells treated with buffer control or 20 μM ABA as well as Col-0 pretreated with 10 μM VAS2870 followed by ABA treatment. Scale bar: 5 μm. B, Violin plots show quantifications of mitochondrial DCF fluorescence following treatment with control buffer, ABA, or pretreated with VAS2870 and then treated with ABA from three separate experiments ($n > 85$). C, Quantification of the mt-roGFP2-Orp1 ratio of the entire guard cell following 20 μM ABA, buffer control, or pretreatment with 10 μM VAS2870 followed by ABA treatment ($n > 77$). All individual values were normalized to the average of the control treatment in Col-0 and are displayed on the graph as blue dots with the median shown in red and lower and upper quartiles indicated in black. *P*-values in black font represent the significance of differences between treatments in the same genotype spanning the compared treatments. *P*-values in blue font represent the significance of differences between *rbohd/f* and Col-0 under the same treatment conditions. *P*-values are recorded according to two-way ANOVA followed by Tukey's post hoc tests.

RBOHF, which were previously reported to function in ABA-induced stomatal closure (Kwak et al., 2003). Figure 7A contains images of DCF fluorescence reported as LUT in Col-0 and the double mutant *rbohd/f*. Not only did the *rbohd/f* double mutant exhibit reduced DCF accumulation in the cytosol (Supplemental Figure 12) following 20 μM ABA treatment for 45 min (as predicted by the known function of RBOH proteins in controlling cytosolic ROS), but we also failed to observe a significant increase in signal within the mitochondria of this mutant (Figure 7B).

We also inhibited RBOH-dependent ROS production with a pharmacological approach. Although diphenylene iodonium (DPI) is a commonly used NADPH oxidase inhibitor that inhibits ABA-dependent guard cell closure in guard cells (Zhang et al., 2001, Gayatri et al., 2017, Watkins et al., 2017), the molecule is a general flavoprotein inhibitor that can directly interfere with metabolic processes in mitochondria (Augsburger et al., 2019). Therefore, we utilized the more selective pan NOX inhibitor, VAS2870, which selectively targets an active-site cysteine that is conserved in mammalian NOX enzymes and plant RBOHs (Yun et al., 2011). We confirmed that VAS2870 regulated ABA responses in guard cells by evaluating its effect on ABA-induced stomatal closure. Pretreatment with 10 μM VAS2870 for 1 h prior to ABA treatment was able to significantly inhibit ABA-dependent stomatal closure compared with guard cells treated with

ABA alone, suggesting it is an effective RBOH inhibitor in guard cells (Supplemental Figure 12, A–B) and supporting the requirement of RBOH activity for full ABA-induced stomatal closure. Preincubation with VAS2870 abolished ABA-induced ROS increases in both the mitochondria (Figure 7B) and the cytosol (Supplemental Figure 12). We also pretreated mt-roGFP2-Orp1 guard cells with VAS2870 and found that the ABA-dependent increases in mitochondrial oxidation seen previously were significantly reduced by inhibitor treatment (Figure 7C). Altogether, these findings indicate that RBOH enzymes play a role in ABA-dependent ROS accumulation in guard cell mitochondria.

## Discussion

Plants regulate the stomatal aperture in response to environmental and hormonal signals through the control of guard cell turgor pressure (Nilson and Assmann, 2007). During drought stress, plants increase ABA synthesis (Muhammad Aslam et al., 2022), which initiates a complex signaling pathway that ultimately leads to stomatal closure (Vishwakarma et al., 2017). Included in this signaling cascade is the activation of RBOH enzymes that trigger a burst of ROS that act as second messengers in guard cell closure (Kwak et al., 2003). The accumulation of ROS in guard cells following ABA treatment has been detected primarily by increases in DCF fluorescence, a nonspecific chemical ROS sensor, with signal quantified across the whole guard cell (Postiglione and Muday, 2020, Pei et al., 2000, Watkins et al., 2017, 2014). However, signaling through ROS is more nuanced, with signaling outputs depending on the type of ROS that is generated and where ROS accumulates (Noctor and Foyer, 2016). Recent technological advances in microscopic resolution and ROS detection (Nietzel et al., 2019, Winterbourn, 2014, Ugalde et al., 2021b), as well as a growing number of genetic resources to disrupt signaling and/or ROS synthesis, allowed us to ask more precise questions about the functions of ROS, including when and where these are made and which ROS function to control signaling and development (Martin et al., 2022). In this study, we use both ROS-responsive fluorescent dyes and genetically encoded biosensors to demonstrate that ABA increases $H_2O_2$ within specific subcellular compartments of guard cells and that these changes are both necessary and sufficient to drive stomatal closure.

We found that ABA significantly increased the fluorescence intensity of the generic ROS probe, DCF, in the cytoplasm, mitochondria, nuclei, and chloroplasts, with the most substantial increases in the mitochondria and chloroplast. The identity of these organelles was verified by linear unmixing of DCF signal from organelle localized dyes and chloroplast autofluorescence. The ABA-induced ROS synthesis in the mitochondria, cytosol, and nucleus was all dependent on the canonical ABA signaling pathway, as the ABA-increased ROS was lost in these organelles in the quintuple ABA receptor mutant *pyl-11458*. However, ABA was still able to trigger a significant increase in the chloroplasts of *pyl-11458*, suggesting alternate mechanisms for ROS generation in this organelle during ABA signaling.

A major component of these ABA-induced ROS is due to increases in $H_2O_2$. We used the $H_2O_2$-selective chemical probe, PO1, and the $H_2O_2$-responsive genetically encoded sensor roGFP2-Orp1, targeted to the cytosol and nucleus, to the mitochondria, or to the chloroplast. This highly reactive biosensor contains a ratiometric readout which provides advantages over chemical dyes due to its self-normalizing output (Gutscher et al., 2009, Ugalde et al., 2021a, Nietzel et al., 2019). This sensor has a cysteine residue that is oxidized by $H_2O_2$ leading to a conformational change that alters its optical properties, resulting in increased signal after excitation at 405 nm and decreased intensity following excitation at 488 nm. Using this sensor, we reveal that ABA treatment leads to a significant increase in $H_2O_2$ when the oxidation ratio in the whole guard cell, cytosol, and nucleus are quantified or when mitochondrial or chloroplast ROS are quantified using the targeted mt-roGFP-Orp1 or plastid-roGFP-Orp1. We also detected ABA-dependent increases in $H_2O_2$ in the chloroplast and in mitochondria with PO1, but not in the cytosol. We stained leaves containing the mitochondrially targeted roGFP2-Orp1 with PO1 and confirmed that the mitochondria labeled with PO1 displayed strong colocalization with mt-roGFP2-Orp1. Together, these experiments reveal ABA-dependent $H_2O_2$ increases in the mitochondria and chloroplasts.

We used several approaches to ask if mitochondrial ROS increases are able to facilitate ABA-dependent stomatal closure. A previous study screened mutants for altered ABA-dependent primary root growth (He et al., 2012, Yang et al., 2014). This approach identified the *abo6* mutant, which was isolated for enhanced ABA response in root cells and had drought tolerance, and elevated ROS within root cells. The mutant gene encoded a DEXH box RNA helicase, which led to the altered synthesis of mitochondrial electron transport proteins; the gene product is localized to the mitochondria of leaf protoplasts (He et al., 2012). The *abo6* mutant had elevated mitochondrial ROS in guard cells with and without ABA treatment and significantly enhanced ABA-induced stomatal closure relative to Col-0. We also observed enhanced ABA-sensitivity in Col-0 guard cells pretreated with mitochondrial complex I inhibitor, rotenone, which also elevates mitochondrial ROS accumulation (Mohammed et al., 2020, Li et al., 2003, Zhou et al., 2014). Rotenone's mechanism of action made this a particularly intriguing finding as the inhibitor increases mitochondrial ROS while limiting oxidative phosphorylation and adenosine triphosphate synthesis (Palmer et al., 1968). This suggests that our findings of increased ABA sensitivity were largely based on the pool of ROS generated in this organelle and not increased energetic requirements.

We also showed that pretreatment with the mitochondrially targeted ROS scavenger, MitoQ (Kelso et al., 2001), significantly blunted mt-roGFP2-Orp1 oxidation and ABA-induced stomatal closure in Col-0 guard cells. As we found

no other reference to MitoQ use in plants, we also asked whether it acted on chloroplasts. Although this compound reduced oxidation of the plastid-roGFP2-Orp1, the effect was smaller than that on mt-roGFP2-Orp1. In particular, MitoQ reduced mt-roGFP2-Orp1 levels to below those of ABA treatment, while plastid-roGFP2-Orp1 was still significantly oxidized by ABA even after MitoQ pretreatment, suggesting MitoQ has mitochondrial selectivity.

Additionally, a previous report demonstrated that impairment of chloroplastic ROS generation through chemical inhibition of photosynthetic electron transport does not have an effect on ABA-induced stomatal closure (Wang et al., 2016). Another study showed that a mutant that lacked chlorophyll in guard cells was still able to close stomata following ABA treatment (Azoulay-Shemer et al., 2015). ABO6 is localized to mitochondria and absent in chloroplast (He et al., 2012), and MitoQ is able to reverse the enhanced ABA stomatal closure phenotype of *abo6* to wild-type levels. Together, these results are consistent with mitochondria as necessary sites of ROS generation for productive ABA signaling in guard cells.

RBOH enzymes were previously implicated in ABA-dependent increases in DCF fluorescence (Kwak et al., 2003, Drerup et al., 2013, Hsu et al., 2018, Postiglione and Muday, 2020) by examination of an *rbohd/rbohf* double mutant (Kwak et al., 2003) and treatment with a RBOH inhibitor, DPI (Watkins et al., 2017), which can also target other enzymes. RBOH enzymes have well-established roles in hormone-induced ROS synthesis in mammals (Vermot et al., 2021) and plants (Chapman et al., 2019). These enzymes produce superoxide in the apoplast, which can be rapidly dismutated into $H_2O_2$ via superoxide dismutase. The influx of $H_2O_2$ into the cytoplasm is facilitated by aquaporins, making it available to reversibly oxidize cytoplasmic protein targets to change their conformation, activity, and/or regulatory properties (Rodrigues et al., 2017, Tian et al., 2016). Yet, whether RBOH enzymes drive ROS accumulation in guard cells in regions beyond the cytoplasm has not been examined.

In guard cells of both an *rbohd/f* double mutant and cells treated with a highly specific pan-RBOH/NOX inhibitor, VAS2870 (Reis et al., 2020), there were reductions in both ABA-induced cytosolic and mitochondrial ROS and ABA-dependent guard cell closure. This suggests a link between RBOH-dependent ROS production and ROS accumulation in guard cell mitochondria. This finding is consistent with a previous report which found that the introduction of the *rbohf* mutation into *abo6* relieved ABA hypersensitivity in *abo6* roots (He et al., 2012). This finding both emphasizes the role of RBOH in ABA-induced ROS in cellular locations beyond the cytosol, such as mitochondria, which is an important insight into the function of this class of signaling-driven, ROS-synthesizing enzymes. Previous work in mammalian systems has shown the ability of NOX enzymes, such as NOX4, to localize to mitochondria (Dikalov, 2011, Shanmugasundaram et al., 2017). However, whether there are RBOHs localized to mitochondria in plants is not currently known.

The regulation of stomatal aperture in response to environmental stimuli, such as drought, is a crucial process in plant adaptation to stress. This study built on prior evidence that ABA drives ROS increases, identified here as $H_2O_2$ as central to this response, as well as revealing the spatial regulation of these ROS. The addition of genetically encoded biosensors to our toolkit of ROS-responsive chemical probes allowed us to overlay the position of ROS accumulation with organelle-specific markers to reveal ABA-elevated ROS in the mitochondria and chloroplast. In support of a function of mitochondrially derived ROS in guard cells, a mutant with increased mitochondrial ROS as well as guard cells with chemically increased mitochondrial ROS production displayed an increased rate of ABA-induced stomatal closure. Meanwhile, a ROS scavenger targeted to this organelle reduced guard cell ABA sensitivity, suggesting ROS production in this organelle functions in the ABA signaling pathway. We also demonstrated that RBOH enzymes play a role in ABA-increased ROS accumulation not only in the cytoplasm but also in guard cell mitochondria. Together, these results indicate that ABA-induced $H_2O_2$ accumulation exhibits tight compartmentalization in organelles such as mitochondria that influences guard cell signaling and physiology.

## Materials and methods

### Plant growth conditions

Arabidopsis (*Arabidopsis thaliana*) seeds that were used include Col-0, *rbohd/rbohf* double mutant (Miller et al., 2009), *pyl1-1*; *pyr1-1*; *pyl4-1*; *pyl5*; *pyl8-1* quintuple mutant (*pyl-11458*) (Antoni et al., 2013) (ABRC), *ABA overly sensitive 6* (*abo6*) (Alonso et al., 2003) (ABRC), GFP-PTS1 reporter (Ramón and Bartel, 2010), roGFP2-Orp1 (Nietzel et al., 2019), plastid-roGFP2-Orp1 (Ugalde et al., 2021a), and mt-roGFP2-Orp1 (Nietzel et al., 2019). Arabidopsis plants were germinated on 1× Murashige and Skoog medium, pH 5.6, Murashige and Skoog vitamins, and 0.8% (w/v) agar, buffered with 0.05% (w/v) MES and supplemented with 1% (w/v) sucrose. After vernalization at 4°C for 48 h, plates were placed under 24-h 120-µmol $m^{-2}$ $s^{-2}$ cool-white light. Seven days after germination, seedlings were transferred to SunGro Redi-Earth Seed Mix. Plants are then grown under a short-day light cycle (8-h light/16-h dark) of 120-µmol $m^{-2}$ $s^{-2}$ cool-white light with relative humidity kept between 60% and 70%. Experiments were conducted on leaves from plants 3 to 4 weeks after germination, unless noted otherwise.

### DCF staining, imaging, and quantification

Chloromethyl 2,7-dihydrodichlorofluorescein diacetate (CM-$H_2$DCF-DA) was dissolved in dimethyl sulfoxide to yield a 50 µM stock. This was diluted in deionized water to yield a final concentration of 4.3 µM with 0.1% (v/v) dimethyl sulfoxide. Epidermal peels of Col-0, *abo6*, or *rbohd/f* were prepared by evenly spraying a microscope slide with a

silicone-based medical adhesive (Hollister stock #7730). After 10 min, the abaxial epidermis of the leaf was pressed into the dried adhesive coat, a drop of water was placed on the leaf surface, and the leaf was gently scraped with a razor blade until only the fixed epidermis remains. Fresh epidermal peels were then fully covered in opening solution (50 mM KCl, and 10 mM MES buffer, pH 6.15) and incubated under cool-white light (120 μmol $m^{-2}$ $s^{-1}$) for 3 h. For VAS2870 treatments, the stomatal opening buffer was then replaced with a stomatal opening solution containing 10 μM VAS2870 for 1 h during the opening process. Epidermal peels were then treated with fresh stomatal opening buffer (control buffer) or a similar solution containing 20 μM ABA for 45 min. Pretreatments were fully removed, and the epidermis was stained for 15 min with 4.3 μM CM $H_2$DCF-DA stain and washed with deionized water. Microscopy was performed on the Zeiss LSM880 LSCM with a 32-detector GaAsP array for spectral unmixing. The Plan Apochromat 63x/1.2NA water objective was used for acquisition. The 488 nm laser line was used to excite the leaf surfaces with 0.4% maximum laser power with a 3.5 digital gain. The gain settings were optimized to produce the maximum DCF signal while preventing oversaturation. All micrographs were acquired using identical offset, gain, and pinhole settings using the same detectors for each experiment. Settings were defined to spectrally separate the DCF and chlorophyll signal by capturing the emission spectrum for each compound in regions in which there was no overlap. Total emission was collected using lambda scanning with a 1 Airy Unit pinhole aperture yielding a 0.9 μm section; the DCF signal alone would later be unmixed from the image for quantification.

Images used for quantification were taken with averaging of 2 with minimal pixel dwell time making sure to limit excess exposure to the laser that may induce ROS. Maximum intensity projections were produced from Z-stacks. The average intensity values within each ROI were acquired, and all values obtained were normalized to the average of each subcellular location under control conditions from three biological replicates with 2–3 technical replicates per experiment. DCF fluorescence intensities were measured in ImageJ by drawing ROIs around the whole stomata, chloroplasts, cytosol, nuclei, and individual mitochondria of multiple guard cells.

The images shown in the figures were captured at high resolution using separate but identically treated samples to those used in the quantification with increased averaging, digital zoom, and pixel dwell time to increase resolution and were not included in any quantification. Individual images were selected that were representative of the magnitude of responses in the images generated for quantification. To produce heat maps, we converted pixel intensities of DCF fluorescence using the look-up tables (LUT) function in the Zen Blue Software.

## PO1 staining, imaging, and quantification

Peroxy Orange 1 (PO1) is an $H_2O_2$ sensor (Dickenson et al., 2010), which was dissolved in dimethyl sulfoxide to yield a 5 mM stock. This was diluted in deionized water to yield a final concentration of 50 μM. Epidermal peels were prepared, and guard cells were fully opened as described earlier, then treated with 20 μM or 100 μM ABA or a control buffer. Pretreatments were fully removed, and the epidermis was stained for 30 min with 50 μM PO1 dye and washed with deionized water. Microscopy was performed using a Zeiss LSM880 LSCM with a 32-detector GaAsP array for spectral unmixing. The Plan Apochromat 63x/1.2NA water objective was used for acquisition. Leaf surfaces were excited with the 488 nm laser line at 0.6% maximum laser power and a digital gain set to 3.5. The gain settings were optimized to produce the maximum PO1 signal while preventing oversaturation. All micrographs were acquired using identical offset, gain, and pinhole settings using the same detectors for each experiment. Settings were defined to spectrally separate the PO1 signal from chlorophyll autofluorescence by capturing the emission spectrum for each compound in regions where only one signal was present. Total emission was then collected using lambda scanning with a 1 Airy Unit pinhole aperture yielding a 0.9 μm section, the spectral signature that was previously calculated as PO1 signal alone was later unmixed from the image for quantification.

Three-dimensional images of PO1 were acquired on the Zeiss LSM880 system equipped with a 32-detector GaAsP array for Airyscan acquisition. Samples were excited with an argon 488 nm laser line using 6% laser power, and a Plan Apochromat 63x/1.2NA water objective was used for image acquisition. Total emission was collected using Airyscan of a z-stack spanning the entire depth of a whole guard cell pair, using the optimal optical slice size calculated by the ZEN Black acquisition software. Images were then rendered in 3D using Aivia image analysis software. x, y and z, y projections were then acquired of cropped regions containing chloroplasts or mitochondria.

To produce heat maps displayed in Figure 2, we converted pixel intensities of PO1 fluorescence using the LUT function in the Zen Blue Software. PO1 fluorescence intensities were measured in ImageJ by drawing ROIs around the chloroplasts, cytosol, nuclei, and individual mitochondria of each guard cell. Due to there being more puncta with bright PO1 fluorescence evident after ABA treatment, as reported previously in tomato (Watkins et al., 2017), we obtained a greater number of data points as ABA concentrations increased. The average intensity values within each ROI were acquired, and all values obtained were normalized to the average of each subcellular location under control conditions from three biological replicates with three technical replicates per experiment.

## Colocalization analysis of ROS chemical probes with mitochondria and peroxisomes

For evaluation of peroxisomal colocalization, Arabidopsis leaves containing PTS1-GFP were peeled and labeled with 50 μM PO1 as described earlier. For evaluation of mitochondrial colocalization, Col-0 Arabidopsis leaves were peeled and

treated with 8.6 μM CM $H_2$DCF-DA as described earlier and then 1 μM Mitotracker Red for 15 min. PTS1-GFP, PO1, and DCF were visualized by exciting leaves excited with the 488 nm laser line at 0.4% maximum laser power, while Mitotracker was visualized through excitation with the 561 nm laser line with laser power set to 0.4%. Each signal was resolved in lambda scanning mode, with emission spectra for each individual spectra being obtained prior to colocalization analysis by imaging single labeled samples. Images were taken at multiple Z-positions, though not combined into maximum intensity projections to not misrepresent colocalization of signals that might be found in the same vertical plane but at different depths. Emission spectra for each signal were then unmixed from corresponding images to better evaluate how either signal contributed to a particular location. For colocalization analysis, samples were examined using the Zeiss Zen colocalization module. The threshold for PO1, GFP-PTS1, DCF, Mitotracker Red, and mt-roGFP2-Orp1 was determined in each image, via regions that contained only one fluorescent signal. Regions of interest surrounding mitochondria in PO1 or DCF were then selected and evaluated for colocalization with GFP-PTS1, mt-roGFP2-Orp1, or Mitotracker Red. Colocalization was then calculated using Pearson's coefficients (weighted colocalization coefficients), and respective scatterplots were generated.

## Imaging and analysis of ROS-sensitive genetically encoded biosensors

Fully mature Arabidopsis rosettes containing roGFP2-Orp1, plastid-roGFP2-Orp1, or mt-roGFP2-Orp1 were excised and peeled prior to being submerged in stomatal opening buffer to equilibrate for 4 h to establish a baseline. For inhibitor treatments, leaf peels were pretreated with stomatal opening buffer containing either 500 nM mitoquinol mesylate (MitoQ) for 3 h or 10 μM VAS2870 for 1 h during the equilibration process. Inhibitor solutions were then removed, rinsed, and replaced with fresh stomatal opening buffer and allowed to incubate until the 4-h opening period was completed. Stomatal opening buffer or inhibitors were then removed following equilibration and replaced with a similar solution containing 20 μM ABA for 0, 15, 30, or 45 min. Microscopy was performed on the Zeiss LSM880 LSCM with a Plan Apochromat 63x/1.2NA water objective was used to sequentially excite leaf surfaces at 405 and 488 nm with 1% maximum laser power. Emission was recorded between 505 and 535 nm to keep autofluorescence at a minimum, with a 2.4 Airy Unit pinhole aperture yielding a 2.0 μm section. We verified that there were no changes in the ratiometric signal calculated with the ABA treatment of Col-0 that was not transformed with this biosensor. Images used for quantification were taken without averaging and with scan speed and pixel dimensions optimized for minimal pixel dwell time in order to limit laser-induced oxidation of the sensor. The Z-slice number was held constant for all image stacks to promote equity of light exposure (and equal photooxidation) across samples. Z-axis profiles of averaged intensity within a 3 $\mu m^2$ spot size were plotted in ImageJ to verify that both fluorescent channels showed alignment of peak intensity values at proximal stack depths. This check was critical to assure the depth alignment of our two distinct fluorescent channels given that we utilized maximum intensity projections for these analyses. The dynamic range of each dye sensor was defined by treating equilibrated samples with 20 mM DTT or 10 mM $H_2O_2$ to determine the maximum reduction or maximum oxidation, respectively.

Images of roGFP2-Orp1 targeted to the cytosol or plastids were captured as described earlier, and maximum intensity projections were analyzed in ImageJ by drawing a region of interest in the nucleus, a cytosolic region, or individual chloroplasts within each guard cell. Images of mt-roGFP2-Orp1 were analyzed by drawing a region of interest around the entire stomata and thresholding to exclude pixels of background intensity values from each measurement. Ratios were calculated by dividing fluorescence intensity following excitation at 405 nm by fluorescence intensity collected after 488-nm excitation. All individual values obtained were normalized to the average of buffer control treated stomata or the 0-min timepoint in the case of time courses. Ratiometric micrographs were generated using the Ratio Redox Analysis MatLab program package (Fricker, 2016).

## Stomatal closure assay

ABA-induced stomatal closure assays were performed with plants 3 to 4 weeks after germination. Epidermal strips were prepared and fully covered in an opening solution as described earlier. For inhibitor treatments, the opening buffer was replaced with a stomatal opening solution containing 50 μM rotenone for 1 h, 500 nM mitoquinol mesylate (MitoQ) for 3 h, or 10 μM VAS2870 for 1 h during the opening process. To induce stomatal closure, the opening buffer was replaced with an equal volume of a similar solution with 20 μM added to induce closure. For quantification of the stomatal aperture, leaf peels were imaged on an ECHO Revolve microscope using transmitted light. Images were acquired using an Olympus UPlanSApochromat 40×/0.95NA objective.

## Statistical analysis

The data for the subcellular localization of DCF and whole stomata roGFP2-Orp1 quantifications were analyzed via Student's *t*-tests using GraphPad Prism 9 comparing ABA to control in each respective cellular location. DCF fluorescence intensities for ABA signaling mutants and widths of stomatal apertures were analyzed using two-way ANOVAs, while subcellular PO1 signal intensity and roGFP2-Orp1 time course data were analyzed by one-way ANOVAs using GraphPad Prism 9. This analysis evaluated differences within genotypes between different treatments and compared genotypes under similar treatments for ABA signaling mutants, between control and multiple ABA treatments for PO1 fluorescence, and between time points for roGFP2-Orp1 and

mt-roGFP2-Orp1. Tukey's multiple comparison tests were then utilized to resolve significant differences between treatments, genotypes, or time points.

### Accession numbers

Sequence data from this article can be found in the GenBank/EMBL data libraries under the accession numbers: *PYR1* (At4g17870), *PYL1* (At5g46790), *PYL4* (At2g38310), *PYL5* (At5g05440), *PYL8* (At5g53160), *ABO6* (At5g04895), *RBOHD* (At5g47910), *RBOHF* (At1g64060).

## Supplemental data

The following materials are available in the online version of this article.

**Supplemental Figure S1**. Abscisic acid (ABA) increases dichlorofluorescein (DCF) fluorescence when entire Arabidopsis guard cells are quantified.

**Supplemental Figure S2**. Reactive oxygen species-sensitive fluorescent probes accumulate in chloroplasts and nuclei.

**Supplemental Figure S3**. There are no significant abscisic acid (ABA)-induced increases in fluorescence of Peroxy Orange 1 (PO1) in the whole stoma, the cytosol, or the nucleus.

**Supplemental Figure S4**. Treatment with hydrogen peroxide ($H_2O_2$) leads to decreased stomatal aperture and elevated Peroxy Orange 1 (PO1) fluorescence.

**Supplemental Figure S5**. Mitochondria have uniform Peroxy Orange 1 (PO1) fluorescence, while chloroplasts have localized regions with the elevated signal.

**Supplemental Figure S6**. Abscisic acid (ABA) treatment alters fluorescence of roGFP2-Orp1 in guard cells consistent with elevated hydrogen peroxide.

**Supplemental Figure S7**. Time course imaging of the same subset of roGFP2-Orp1 stomata can result in sensor oxidation even under control conditions.

**Supplemental Figure S8**. A 45-min abscisic acid (ABA) treatment results in an increased oxidation ratio of mt-roGFP2-Orp1.

**Supplemental Figure S9**. Peroxy Orange (PO1) and mt-roGFP2-Orp1 colocalize consistent with abscisic acid-induced reactive oxygen species in mitochondria.

**Supplemental Figure S10**. Abscisic acid treatment increased the oxidation of plastid-roGFP2-Orp1.

**Supplemental Figure S11**. The abscisic acid (ABA)-induced oxidation of plastid-roGFP2-Orp1 is reduced by pretreatment with MitoQ.

**Supplemental Figure S12**. The respiratory burst oxidase homolog (RBOH)-selective inhibitor VAS2870 reduces abscisic acid (ABA)-dependent guard cell closure and dichlorofluorescein (DCF) accumulation.

## Acknowledgments

We would like to acknowledge the assistance of Dr Heather Brown Harding (Microscopy core facility) with imaging. We thank Dr Leslie Poole for her generous sharing of expertise and research material. We also thank Antipodean Pharmaceuticals, Inc for supplying mitoquinol mesylate (MitoQ). We greatly appreciate the generosity of Dr Andreas Meyer and Dr Jose Ugalde in sharing roGFP2-Orp1, plastid-roGFP2-Orp1, and mt-roGFP2-Orp1 seeds, as well as providing helpful feedback on an early draft of the manuscript. We also thank Dr Gad Miller for providing *rbohd/f* seeds and Dr Bonnie Bartel for the GFP-PTS1 transgenic line, and the ABRC for distributing *pyl-11458* and *abo6* seeds. Lastly, we would like to thank members of the Muday lab for their valuable input on the manuscript.

## Funding

This work was funded by NSF IOS-1558046 to G.K.M and a fellowship from the Wake Forest University's Center for Molecular Signaling and an NIH T32 GM127261 fellowship to A.E.P. The content is solely the responsibility of the authors and does not necessarily represent the official view of the National Institutes of Health.

*Conflict of interest statement:* The authors declare that the research was conducted without any known commercial or financial interests that would serve as a potential conflict of interest.

## References

**Alonso JM, Stepanova AN, Leisse TJ, Kim CJ, Chen H, Shinn P, Stevenson DK, Zimmerman J, Barajas P, Cheuk R, et al.** (2003) Genome-wide insertional mutagenesis of *Arabidopsis thaliana*. Science **301**(5633): 653–657

**An Y, Liu L, Chen L, Wang L** (2016) ALA inhibits ABA-induced stomatal closure via reducing $H_2O_2$ and Ca2+ levels in guard cells. Front Plant Sci **7**: 482

**Antoni R, Gonzalez-Guzman M, Rodriguez L, Peirats-Llobet M, Pizzio GA, Fernandez MA, De Winne N, De Jaeger G, Dietrich D, Bennett MJ, et al.** (2013) PYRABACTIN RESISTANCE1-LIKE8 plays an important role for the regulation of abscisic acid signaling in root. Plant Physiol **161**(2): 931–941

**Augsburger F, Filippova A, Rasti D, Seredenina T, Lam M, Maghzal G, Mahiout Z, Jansen-Dürr P, Knaus UG, Doroshow J, et al.** (2019) Pharmacological characterization of the seven human NOX isoforms and their inhibitors. Redox Biol **26**: 101272

**Azoulay-Shemer T, Palomares A, Bagheri A, Israelsson-Nordstrom M, Engineer CB, Bargmann BO, Stephan AB, Schroeder JI** (2015) Guard cell photosynthesis is critical for stomatal turgor production, yet does not directly mediate $CO_2$—and ABA-induced stomatal closing. Plant J **83**(4): 567–581

**Babbar R, Karpinska B, Grover A, Foyer CH** (2021) Heat-induced oxidation of the nuclei and cytosol. Front Plant Sci **11**: 617779

**Bienert GP, Moller AL, Kristiansen KA, Schulz A, Moller IM, Schjoerring JK, Jahn TP** (2007) Specific aquaporins facilitate the diffusion of hydrogen peroxide across membranes. J Biol Chem **282**(2): 1183–1192

**Chapman JM, Muhlemann JK, Gayomba SR, Muday GK** (2019) RBOH-dependent ROS synthesis and ROS scavenging by plant specialized metabolites to modulate plant development and stress responses. Chem Res Toxicol **32**(3): 370–396

**Demidchik V** (2018) ROS-Activated ion channels in plants: biophysical characteristics, physiological functions and molecular nature. Int J Mol Sci **19**(4): 1263

**Dickinson BC, Huynh C, Chang CJ** (2010) A palette of fluorescent probes with varying emission colors for imaging hydrogen peroxide signaling in living cells. J Am Chem Soc **132**(16): 5906–5915

**Dikalov S** (2011) Cross talk between mitochondria and NADPH oxidases. Free Radic Biol Med **51**(7): 1289–1301

**Drerup MM, Schlücking K, Hashimoto K, Manishankar P, Steinhorst L, Kuchitsu K, Kudla J** (2013) The calcineurin B-like calcium sensors CBL1 and CBL9 together with their interacting protein kinase CIPK26 regulate the Arabidopsis NADPH oxidase RBOHF. Mol Plant **6**(2): 559–569

**Fahad S, Bajwa AA, Nazir U, Anjum SA, Farooq A, Zohaib A, Sadia S, Nasim W, Adkins S, Saud S, et al.** (2017) Crop production under drought and heat stress: plant responses and management options. Front Plant Sci **8**: 1147

**Fricker MD** (2016) Quantitative redox imaging software. Antioxid Redox Signal **24**(13): 752–762

**Fukai T, Ushio-Fukai M** (2011) Superoxide dismutases: role in redox signaling, vascular function, and diseases. Antioxid Redox Signal **15**(6): 1583–1606

**Gadjev I, Vanderauwera S, Gechev TS, Laloi C, Minkov IN, Shulaev V, Apel K, Inzé D, Mittler R, Van Breusegem F** (2006) Transcriptomic footprints disclose specificity of reactive oxygen species signaling in Arabidopsis. Plant Physiol **141**(2): 436–445

**Gayatri G, Agurla S, Kuchitsu K, Anil K, Podile AR, Raghavendra AS** (2017) Stomatal closure and rise in ROS/NO of Arabidopsis guard cells by tobacco microbial elicitors: cryptogein and harpin. Front Plant Sci **8**: 1096

**Geiger D, Scherzer S, Mumm P, Stange A, Marten I, Bauer H, Ache P, Matschi S, Liese A, Al-Rasheid KAS, et al.** (2009) Activity of guard cell anion channel SLAC1 is controlled by drought-stress signaling kinase-phosphatase pair. Proc Natl Acad Sci USA **106**(50): 21425–21430

**Gutscher M, Sobotta MC, Wabnitz GH, Ballikaya S, Meyer AJ, Samstag Y, Dick TP** (2009) Proximity-based protein thiol oxidation by $H_2O_2$-scavenging peroxidases. J Biol Chem **284**(46): 31532–31540

**Halliwell B, Whiteman M** (2004) Measuring reactive species and oxidative damage in vivo and in cell culture: how should you do it and what do the results mean? Br J Pharmacol **142**(2): 231–255

**He J, Duan Y, Hua D, Fan G, Wang L, Liu Y, Chen Z, Han L, Qu LJ, Gong Z** (2012) DEXH Box RNA helicase-mediated mitochondrial reactive oxygen species production in Arabidopsis mediates crosstalk between abscisic acid and auxin signaling. Plant Cell **24**(5): 1815–1833

**Hsu P-K, Dubeaux G, Takahashi Y, Schroeder JI** (2021) Signaling mechanisms in abscisic acid-mediated stomatal closure. Plant J **105**(2): 307–321

**Hsu P-K, Takahashi Y, Munemasa S, Merilo E, Laanemets K, Waadt R, Pater D, Kollist H, Schroeder JI** (2018) Abscisic acid-independent stomatal $CO_2$ signal transduction pathway and convergence of $CO_2$ and ABA signaling downstream of OST1 kinase. Proc Natl Acad Sci USA **115**(42): E9971–E9980

**Jezek M, Blatt MR** (2017) The membrane transport system of the guard cell and its integration for stomatal dynamics. Plant Physiol **174**(2): 487–519

**Kalyanaraman B, Darley-Usmar V, Davies KJA, Dennery PA, Forman HJ, Grisham MB, Mann GE, Moore K, Roberts LJ, Ischiropoulos H** (2012) Measuring reactive oxygen and nitrogen species with fluorescent probes: challenges and limitations. Free Radic Biol Med **52**(1): 1–6

**Kelso GF, Porteous CM, Coulter CV, Hughes G, Porteous WK, Ledgerwood EC, Smith RAJ, Murphy MP** (2001) Selective targeting of a redox-active ubiquinone to mitochondria within cells: aNTIOXIDANT AND ANTIAPOPTOTIC PROPERTIES *. J Biol Chem **276**(7): 4588–4596

**Klejchova M, Silva-Alvim FAL, Blatt MR, Alvim JC** (2021) Membrane voltage as a dynamic platform for spatiotemporal signaling, physiological, and developmental regulation. Plant Physiol **185**(4): 1523–1541

**Kwak JM, Mori IC, Pei ZM, Leonhardt N, Torres MA, Dangl JL, Bloom RE, Bodde S, Jones JD, Schroeder JI** (2003) NADPH Oxidase AtrbohD and AtrbohF genes function in ROS-dependent ABA signaling in Arabidopsis. EMBO J **22**(11): 2623–2633

**Lamaoui M, Jemo M, Datla R, Bekkaoui F** (2018) Heat and drought stresses in crops and approaches for their mitigation. Front Chem **6**: 26

**Leshem Y, Levine A** (2013) Zooming into sub-organellar localization of reactive oxygen species in guard cell chloroplasts during abscisic acid and methyl jasmonate treatments. Plant Signal Behav **8**(10): e25689

**Li N, Ragheb K, Lawler G, Sturgis J, Rajwa B, Melendez JA, Robinson JP** (2003) Mitochondrial complex I inhibitor rotenone induces apoptosis through enhancing mitochondrial reactive oxygen species production*. J Biol Chem **278**(10): 8516–8525

**Li Q, Wang Y-J, Liu C-K, Pei Z-M, Shi W-L** (2017) The crosstalk between ABA, nitric oxide, hydrogen peroxide, and calcium in stomatal closing of Arabidopsis thaliana. Biologia **72**(10): 1140–1146

**Ma Y, Szostkiewicz I, Korte A, Moes D, Yang Y, Christmann A, Grill E** (2009) Regulators of PP2C phosphatase activity function as abscisic acid sensors. Science **324**(5930): 1064–1068

**Martin RE, Postiglione AE, Muday GK** (2022) Reactive oxygen species function as signaling molecules in controlling plant development and hormonal responses. Curr Opin Plant Biol **69**: 102293

**Miller G, Schlauch K, Tam R, Cortes D, Torres MA, Shulaev V, Dangl JL, Mittler R** (2009) The plant NADPH oxidase RBOHD mediates rapid systemic signaling in response to diverse stimuli. Sci Signal **2**(84): ra45

**Mohammed F, Gorla M, Bisoyi V, Tammineni P, Sepuri NBV** (2020) Rotenone-induced reactive oxygen species signal the recruitment of STAT3 to mitochondria. FEBS Lett **594**(9): 1403–1412

**Muhammad Aslam M, Waseem M, Jakada BH, Okal EJ, Lei Z, Saqib HSA, Yuan W, Xu W, Zhang Q** (2022) Mechanisms of abscisic acid-mediated drought stress responses in plants. Int J Mol Sci **23**(3): 1084

**Nietzel T, Elsässer M, Ruberti C, Steinbeck J, Ugalde JM, Fuchs P, Wagner S, Ostermann L, Moseler A, Lemke P, et al.** (2019) The fluorescent protein sensor roGFP2-Orp1 monitors in vivo $H_2O_2$ and thiol redox integration and elucidates intracellular $H_2O_2$ dynamics during elicitor-induced oxidative burst in Arabidopsis. New Phytologist **221**(3): 1649–1664

**Nilson SE, Assmann SM** (2007) The control of transpiration. Insights from Arabidopsis. Plant Physiol **143**(1): 19–27

**Nishimura N, Sarkeshik A, Nito K, Park S-Y, Wang A, Carvalho PC, Lee S, Caddell DF, Cutler SR, Chory J, et al.** (2010) PYR/PYL/RCAR family members are major in-vivo ABI1 protein phosphatase 2C-interacting proteins in Arabidopsis. Plant J **61**(2): 290–299

**Noctor G, Foyer CH** (2016) Intracellular redox compartmentation and ROS-related communication in regulation and signaling. Plant Physiol **171**(3): 1581–1592

**Palmer G, Horgan DJ, Tisdale H, Singer TP, Beinert H** (1968) Studies on the respiratory chain-linked reduced nicotinamide adenine dinucleotide dehydrogenase. XIV. Location of the sites of inhibition of rotenone, barbiturates, and piericidin by means of electron paramagnetic resonance spectroscopy. J Biol Chem **243**(4): 844–847

**Park SY, Fung P, Nishimura N, Jensen DR, Fujii H, Zhao Y, Lumba S, Santiago J, Rodrigues A, Chow TF, et al.** (2009) Abscisic acid inhibits type 2C protein phosphatases via the PYR/PYL family of START proteins. Science **324**(5930): 1068–1071

**Pei ZM, Murata Y, Benning G, Thomine S, Klusener B, Allen GJ, Grill E, Schroeder JI** (2000) Calcium channels activated by hydrogen peroxide mediate abscisic acid signalling in guard cells. Nature **406-**(6797): 731–734

**Postiglione AE, Muday GK** (2020) The role of ROS homeostasis in ABA-induced guard cell signaling. Front Plant Sci **11**: 968

**Qi J, Song C-P, Wang B, Zhou J, Kangasjärvi J, Zhu J-K, Gong Z** (2018) Reactive oxygen species signaling and stomatal movement in plant

responses to drought stress and pathogen attack. J Integr Plant Biol **60**(9): 805–826

**Qu Y, Song P, Hu Y, Jin X, Jia Q, Zhang X, Chen L, Zhang Q** (2018) Regulation of stomatal movement by cortical microtubule organization in response to darkness and ABA signaling in Arabidopsis. Plant Growth Regul **84**(3): 467–479

**Ramón NM, Bartel B** (2010) Interdependence of the peroxisome-targeting receptors in Arabidopsis thaliana: PEX7 facilitates PEX5 accumulation and import of PTS1 cargo into peroxisomes. Mol Biol Cell **21**(7): 1263–1271

**Reis J, Massari M, Marchese S, Ceccon M, Aalbers FS, Corana F, Valente S, Mai A, Magnani F, Mattevi A** (2020) A closer look into NADPH oxidase inhibitors: validation and insight into their mechanism of action. Redox Biol **32**: 101466

**Rodrigues O, Reshetnyak G, Grondin A, Saijo Y, Leonhardt N, Maurel C, Verdoucq L** (2017) Aquaporins facilitate hydrogen peroxide entry into guard cells to mediate ABA- and pathogen-triggered stomatal closure. Proc Natl Acad Sci USA **114**(34): 9200–9205

**Scuffi D, Nietzel T, Di Fino LM, Meyer AJ, Lamattina L, Schwarzländer M, Laxalt AM, García-Mata C** (2018) Hydrogen sulfide increases production of NADPH oxidase-dependent hydrogen peroxide and phospholipase D-derived phosphatidic acid in guard cell signaling. Plant Physiol **176**(3): 2532–2542

**Shanmugasundaram K, Nayak BK, Friedrichs WE, Kaushik D, Rodriguez R, Block K** (2017) NOX4 functions as a mitochondrial energetic sensor coupling cancer metabolic reprogramming to drug resistance. Nat Commun **8**(1): 997

**Sirichandra C, Gu D, Hu HC, Davanture M, Lee S, Djaoui M, Valot B, Zivy M, Leung J, Merlot S, et al.** (2009) Phosphorylation of the Arabidopsis AtrbohF NADPH oxidase by OST1 protein kinase. FEBS Lett **583**(18): 2982–2986

**Suzuki N, Miller G, Morales J, Shulaev V, Torres MA, Mittler R** (2011) Respiratory burst oxidases: the engines of ROS signaling. Curr Opin Plant Biol **14**(6): 691–699

**Swanson SJ, Choi WG, Chanoca A, Gilroy S** (2011) In vivo imaging of Ca2+, pH, and reactive oxygen species using fluorescent probes in plants. Annu Rev Plant Biol **62**(1): 273–297

**Takahashi Y, Zhang J, Hsu P-K, Ceciliato PHO, Zhang L, Dubeaux G, Munemasa S, Ge C, Zhao Y, Hauser F, et al.** (2020) MAP3Kinase-dependent SnRK2-kinase activation is required for abscisic acid signal transduction and rapid osmotic stress response. Nat Commun **11**(1): 12

**Tian S, Wang X, Li P, Wang H, H JI, Xie J, Qiu Q, Shen D, Dong H** (2016) Plant aquaporin AtPIP1; 4 links apoplastic $H_2O_2$ induction to disease immunity pathways. Plant Physiol **171**(3): 1635–1650

**Tõldsepp K, Zhang J, Takahashi Y, Sindarovska Y, Hõrak H, Ceciliato PHO, Koolmeister K, Wang Y-S, Vaahtera L, Jakobson L, et al.** (2018) Mitogen-activated protein kinases MPK4 and MPK12 are key components mediating $CO_2$-induced stomatal movements. Plant J **96**(5): 1018–1035

**Ugalde JM, Fuchs P, Nietzel T, Cutolo EA, Homagk M, Vothknecht UC, Holuigue L, Schwarzländer M, Müller-Schüssele SJ, Meyer AJ** (2021a) Chloroplast-derived photo-oxidative stress causes changes in $H_2O_2$ and EGSH in other subcellular compartments. Plant Physiol **186**(1): 125–141

**Ugalde JM, Schlößer M, Dongois A, Martinière A, Meyer AJ** (2021b) The latest HyPe(r) in plant $H_2O_2$ biosensing. Plant Physiol **187**(2): 480–484

**Vermot A, Petit-Härtlein I, Smith SME, Fieschi F** (2021) NADPH Oxidases (NOX): an overview from discovery, molecular mechanisms to physiology and pathology. Antioxidants (Basel, Switzerland) **10**(6): 890

**Vishwakarma K, Upadhyay N, Kumar N, Yadav G, Singh J, Mishra RK, Kumar V, Verma R, Upadhyay RG, Pandey M, et al.** (2017) Abscisic acid signaling and abiotic stress tolerance in plants: a review on current knowledge and future prospects. Front Plant Sci **8**: 161

**Wang WH, He EM, Chen J, Guo Y, Chen J, Liu X, Zheng HL** (2016) The reduced state of the plastoquinone pool is required for chloroplast-mediated stomatal closure in response to calcium stimulation. Plant J **86**(2): 132–144

**Watkins JM, Chapman JM, Muday GK** (2017) Abscisic acid-induced reactive oxygen species are modulated by flavonols to control stomata aperture. Plant Physiol **175**(4): 1807–1825

**Watkins JM, Hechler PJ, Muday GK** (2014) Ethylene-induced flavonol accumulation in guard cells suppresses reactive oxygen species and moderates stomatal aperture. Plant Physiol **164**(4): 1707–1717

**Winterbourn CC** (2014) The challenges of using fluorescent probes to detect and quantify specific reactive oxygen species in living cells. Biochim Biophys Acta **1840**(2): 730–738

**Wu X, Qiao Z, Liu H, Acharya BR, Li C, Zhang W** (2017) CML20, an Arabidopsis calmodulin-like protein, negatively regulates guard cell ABA signaling and drought stress tolerance. Front Plant Sci **8**: 824

**Xu Z, Jiang Y, Jia B, Zhou G** (2016) Elevated-$CO_2$ response of stomata and its dependence on environmental factors. Front Plant Sci **7**: 657

**Yang L, Zhang J, He J, Qin Y, Hua D, Duan Y, Chen Z, Gong Z** (2014) ABA-mediated ROS in mitochondria regulate root meristem activity by controlling PLETHORA expression in Arabidopsis. PLoS Genet **10**-(12): e1004791

**Yun B-W, Feechan A, Yin M, Saidi NBB, Le Bihan T, Yu M, Moore JW, Kang J-G, Kwon E, Spoel SH, et al.** (2011) S-nitrosylation of NADPH oxidase regulates cell death in plant immunity. Nature **478**(7368): 264–268

**Zhang L, Takahashi Y, Hsu P-K, Kollist H, Merilo E, Krysan PJ, Schroeder JI** (2020) FRET Kinase sensor development reveals SnRK2/OST1 activation by ABA but not by MeJA and high $CO_2$ during stomatal closure. Elife **9**: e56351

**Zhang X, Zhang L, Dong F, Gao J, Galbraith DW, Song CP** (2001) Hydrogen peroxide is involved in abscisic acid-induced stomatal closure in Vicia faba. Plant Physiol **126**(4): 1438–1448

**Zhou Q, Liu C, Liu W, Zhang H, Zhang R, Liu J, Zhang J, Xu C, Liu L, Huang S, et al.** (2014) Rotenone induction of hydrogen peroxide inhibits mTOR-mediated S6K1 and 4E-BP1/eIF4E pathways, leading to neuronal apoptosis. Toxicol Sci **143**(1): 81–96